Higher-intensity ultrasound accelerates fracture healing via mechanosensitive ion channel Piezo1

Inoue, Shota ; Li, Changxin ; Hatakeyama, Junpei ; Jiang, Hanlin ; Kuroki, Hiroshi ; Moriyama, Hideki

(Citation)
Bone,177:116916

(Issue Date)
2023-12

(Resource Type)
journal article

(Version)
Accepted Manuscript

Higher-intensity ultrasound accelerates fracture healing via mechanosensitive ion channel Piezo1

Running title: Ultrasound accelerates fracture healing

Shota Inoue [a], Changxin Li [a], Junpei Hatakeyama [a, b], Hanlin Jiang [a], Hiroshi Kuroki [c], Hideki Moriyama PhD [d*]

[a] Department of Rehabilitation Science, Graduate School of Health Sciences, Kobe University, Kobe, Japan
[b] Research Fellowship of the Japan Society for the Promotion of Science
[c] Department of Physical Therapy, Human Health Sciences, Graduate School of Medicine, Kyoto University, Kyoto, Japan.
[d] Life and Medical Sciences Area, Health Sciences Discipline, Kobe University, Kobe, Japan

[*]**Correspondence:**
Hideki MORIYAMA, Ph.D.
Professor
Life and Medical Sciences Area, Health Sciences Discipline, Kobe University
Tomogaoka 7-10-2, Suma-ku, Kobe, Hyogo, 654-0142, Japan
Tel & Fax +81 78 796 4574
E-mail morihide@harbor.kobe-u.ac.jp

Abstract

Osteoporosis-related fractures are a major public health problem. Mechanobiological stimulation utilizing low-intensity pulsed ultrasound (LIPUS) is the most widely accepted modality for accelerating fracture healing. However, recent evidence has demonstrated the ineffectiveness of LIPUS, and the biophysical mechanisms of ultrasound-induced bone formation also remain elusive. Here, we demonstrate that ultrasound at a higher intensity than LIPUS effectively accelerates fracture healing in a mouse osteoporotic fracture model. Higher-intensity ultrasound promoted chondrogenesis and hypertrophic differentiation of chondrocytes in the fracture callus. Higher-intensity ultrasound also increased osteoblasts and newly formed bone in the callus, resulting in accelerated endochondral ossification during fracture healing. In addition, we found that accelerated fracture healing by ultrasound exposure was attenuated when the mechanosensitive ion channel Piezo1 was inhibited by GsMTx4. Ultrasound-induced new bone formation in the callus was attenuated in fractured mice treated with GsMTx4. Similar results were also confirmed in a 3D osteocyte-osteoblast co-culture system, where osteocytic Piezo1 knockdown attenuated the expression of osteoblastic genes after ultrasound exposure. Together these results demonstrate that higher-intensity ultrasound than clinically used LIPUS can accelerate endochondral ossification after fractures. Furthermore, our results suggest that mechanotransduction via Piezo1 mediates ultrasound-stimulated fracture healing and bone formation.

Keywords: Ultrasound, Fracture, Osteocytes, Osteoblasts, Piezo1

1. Introduction

Fractures are the most common traumatic injury in humans [1]. Osteoporosis-related fractures require long-term medical management resulting in prolonged immobility and increased morbidity, mortality, and healthcare costs [2,3]. Therefore, therapeutic strategies to accelerate fracture healing are critical for patients.

Low-intensity pulsed ultrasound (LIPUS) is acoustic waves with an intensity < 0.1 W/cm^2 that has been shown to accelerate fracture healing [4,5]. Although LIPUS has been widely approved for fracture healing in clinical practice, a recent large-scale TRUST trial [6] and a systematic review and meta-analysis of randomized controlled trials [7] reported no positive effect of LIPUS on radiographic fracture healing. Many others have also demonstrated the ineffectiveness of LIPUS in fracture healing in clinical [8,9] and animal studies [10,11], raising doubts about its therapeutic utility. We have previously hypothesized that the lack of efficacy of LIPUS may be due to its intensity and have verified that ultrasound of a higher intensity than LIPUS accelerates bone defect healing in rats [12]. Additionally, other studies including ours have shown that ultrasound attenuates bone loss in estrogen deficiency in an intensity-dependent manner [13,14], and higher-intensity ultrasound may have a high osteogenic potential. However, unlike our previous bone defect model, which heals only by intramembranous ossification [12], human transverse fractures heal by endochondral ossification, a complex healing process involving inflammation, chondrogenesis, callus formation, and remodeling [1]. Therefore, our previous experiments did not allow us to reliably support benefit with higher-intensity ultrasound. Several studies have reported the intensity-dependent effects of ultrasound on the cellular responses necessary for endochondral ossification, including cell proliferation [12] and chondrogenic [15,16] and osteogenic [17] differentiation of mesenchymal stem cells. Thus, the fracture healing response to ultrasound may vary with its intensity, and how higher-intensity ultrasound than LIPUS affects endochondral ossification remains unclear.

The lack of consensus on the efficacy of LIPUS in fracture healing may be due to a poor understanding of its biophysical mechanism. The understanding of the mechanism underlying ultrasound-induced bone formation focuses primarily on the osteoblastic response. Earlier, *in vitro* studies have shown that LIPUS promotes osteoblastic bone formation by increasing the production of cyclo-oxygenase 2 and prostaglandin E2 [18,19]. On the other hand, for the ultrasound to have a biological effect, its mechanical waves, delivered transcutaneously to the fracture site, must be converted into a biochemical signal

inside the cells. Osteocytes are the main mechanosensory cells in bone, converting the mechanical signals into biochemical signals to the effector cells (ie, osteoblasts and osteoclasts) via secreted factors such as sclerostin, FGF-23, and RANKL [20]. Osteocytes have also been recognized as playing an important role in fracture healing [21]. The role of osteocytes in ultrasound response, however, is poorly understood. Previous studies have shown that conditioned media from ultrasound-stimulated osteocytes promotes osteoblast differentiation [22] and that ultrasound does not affect fracture healing in medaka, whose bones lack osteocytes [23]. Moreover, our previous study indicated that osteocytic sclerostin expression was downregulated only by higher-intensity ultrasound in rat cortical bone, but not by the intensity of LIPUS [12]. Taken together, osteocytes may be involved in osteoblastic bone formation in response to ultrasound; however, the biological mechanism underlying ultrasound sensing and ultrasound-induced mechanotransduction between osteocytes and osteoblasts remains to be elucidated. Given the importance of osteocytes in fracture healing, understanding the biological mechanism of ultrasound-induced osteogenesis centered on osteocytes, which cannot be revealed by *in vitro* studies focused on osteoblasts [18,19], allows for the identification of an effective approach to fractures.

Ultrasonic mechanical signals have been proposed to be transmitted to biochemical signals in the cell by mechanosensitive protein integrins [18,19]. Alternatively, the mechanosensitive ion channel Piezo1 has been shown to play a crucial role in mechanotransduction in osteoblasts and osteocytes and is a key determinant of bone homeostasis and metabolism [24–26]. In addition, a series of studies have reported that Piezo1 is essential for mechanotransduction of the ultrasound responses in umbilical vein endothelial cells [27], cortical neurons [28], dental stem cells [29], and pre-osteoblastic cells [30]. Mechanosensation by Piezo1 is also important for the fracture healing process [31,32]. However, whether Piezo1 is involved in the processes of ultrasound-associated mechanotransduction in osteocytes and ultrasound-stimulated fracture healing remains unclear.

This study aimed to clarify the effects of higher-intensity ultrasound than LIPUS on fracture healing and the mechanism of ultrasound sensing in bone and ultrasound-stimulated bone formation. To achieve our goal, we evaluated the effects of different ultrasound intensities on endochondral ossification in a mouse osteoporotic fracture model. We further established a 3D osteocyte-osteoblast co-culture system and examined the effects of ultrasound on osteocyte mechanotransduction.

2. Materials and Methods

2.1. Experimental design and animal care

Female (n = 92, 8-week-old) and male (n = 24, 12-week-old) C57BL/6J mice were purchased from Japan SLC (Shizuoka, Japan). Animals were housed in plastic cages with bedding and were maintained under artificially controlled conditions at a temperature of 22 ± 1°C with humidity of 55 ± 5% and a 12-hour light/12-hour dark cycle with access to water and food *ad libitum*. All experimental procedures were approved by the Institutional Animal Care and Use Committee and performed according to the Animal Experimentation Regulations of Kobe University (approval number: P210802).

All female mice were subjected to bilateral ovariectomy to simulate postmenopausal osteoporosis. The success of ovariectomy was confirmed by measuring uterine wet weight at the end of the experimental period. Four weeks after the ovariectomy, a standard transverse mid-shaft femoral fracture was created as previously described [33]. Briefly, mice were anesthetized with 4 mg/kg midazolam, 0.75 mg/kg medetomidine hydrochloride, and 5 mg/kg butorphanol tartrate medetomidine. A 0.1 mm tungsten guide wire was inserted into the left femoral intramedullary canal, and a closed mid-shaft fracture was created using the three-point bending method. A 25-gauge needle was inserted over the guide wire to stabilize the fractured femur. The mice were then randomly divided into the following 3 groups: untreated after fracture (control group), treated with ultrasound at intensities of 0.04 W/cm^2 (US-0.04 W group) or 0.2 W/cm^2 (US-0.2 W group) after the fracture. Mice in the treatment groups received ultrasound for 20 min/day, 7 days/week starting from day 1 after the fracture. Mice were euthanized at 7, 14, 21, and 28 days post-fracture (n = 7-8 mice/group/time point) and the femurs were collected.

For the *in vivo* Piezo1 inhibition experiments, the male mice underwent the same femoral fracture at 12 weeks of age and were divided into the vehicle, vehicle + US, GsMTx4, and GsMTx4 + US groups (n = 5-6 mice/group). Male mice were selected to avoid the effects of sex hormones on mechanotransduction in bone [34]. Mice were injected intraperitoneally with vehicle control (saline) or 1 mg/kg GsMTx4 (A16103; AdooQ BioScience, Irvine, CA, USA) dissolved in saline every day from the first day after the fracture. Mice in the vehicle + US and GsMTx4 + US groups were exposed to the ultrasound at an intensity of 0.2 W/cm^2 for 20 min/day, 7 days/week. The fractured femurs were collected 14 days after the fracture.

2.2. In vivo ultrasound exposure

The fractured femurs in the US groups were exposed to an ultrasound stimulation for 20 min/day, 7 days/week. Mice were anesthetized with isoflurane and placed in the right lateral decubitus position. The ultrasound transducer (3.3 cm in diameter) with the ultrasound device (ULTRASON RE-3000; Nihon Medix, Chiba, Japan) was then placed at the center of the fracture site from the lateral side of the femur in all mice. To maximize the coupling of the transducer to the skin surface, the hindlimbs were shaved and the ultrasound gels were applied between the skin and the ultrasound transducer. The ultrasound was delivered with a pulse width of 200 μs of a 1.5 MHz sine wave with a repetition frequency of 1 kHz and spatial-averaged temporal averaged intensity (I_{SATA}) of 0.04 or 0.2 W/cm^2. Mice in the untreated groups were similarly anesthetized and received sham treatment in which the transducer and ultrasound gels were applied without emitting ultrasound.

2.3. Micro-computed tomography (μCT)

At the end of the experimental period, the fractured femurs were harvested and scanned using a micro 3D X-ray CT system (R_mCT2; Rigaku, Tokyo, Japan) with an isotropic voxel resolution of 10 μm, operating at a voltage of 90 kV, current of 160 μA, and a scan time of 180 seconds. 3D image reconstruction and data processing were completed with TRI/3D-BON software (Ratoc, Tokyo, Japan), and a 4.5-mm region of interest (ROI; 2.25 mm proximal and distal to the fracture gap) was used for the subsequent analyses. Mineralized tissue was distinguished from the air and soft tissue by a threshold of 394.8 mg HA/cm^3 [35]. Bone mineral density (BMD) and bone volume fraction (BV/TV) were determined within the fracture callus ROIs using TRI/3D-BON script.

2.4. Mechanical testing

On day 28 post-fracture, the mechanical properties of the fractured femurs were assessed by a three-point bending test using a mechanical testing device (AUTOGRAPH, Shimadzu, Kyoto, Japan). The femur was placed anteriorly on two lower support bars 8 mm apart. A constant load was then applied to the fracture site at a displacement rate of 10 mm/min until failure. The resulting force and displacement data were analyzed to determine the ultimate load and energy to failure.

2.5. Histology

2.5.1. Histological preparation

Non-demineralized frozen sections were prepared according to the Kawamoto method [36]. Briefly, the femurs on days 7, 14, and 21 post-fracture were freeze-embedded with a super cryo-embedding medium (SCEM, Leica Microsystems, Tokyo, Japan) in isopentane at -75°C. The frozen block was cut into 5-µm sagittal sections at a central point with the largest callus area in the bone.

2.5.2. Histomorphometric analysis

Following a previous study [37], the fibrous, cartilaginous, and newly formed bone areas in the total fracture callus were measured on digitized images of Safranin O/Fast green-stained sections and alcian blue/picrosirius red-stained sections using Fiji/ImageJ. The degree of fracture healing was also scored on the same Safranin O-stained sections using the five-point scale based on a previously described method [38]. To detect alkaline phosphatase (ALP) and tartrate-resistant acid phosphatase (TRAP), sections were stained with a TRAP/ALP staining kit (Wako Pure Chemical, Osaka, Japan) according to the manufacturer's instructions. ALP- or TRAP-stained sections were color segmented using the color deconvolution plug-in built into Fiji/ImageJ [39]. The ALP- or TRAP-positive areas in the total callus were identified by Fiji/ImageJ on the segmented color images using a specific threshold. The positive area per total callus area was calculated.

2.5.3. Immunohistochemistry

According to protocols established in our laboratory [14,40], sections were immunostained against type II collagen (diluted 1:400, SAB4500366; Sigma Aldrich, St. Louis, MO, USA) and type X collagen (diluted 1:10000, LB-0092; LSL, Tokyo, Japan). A subsequent reaction was made by the streptavidin-biotin-peroxidase complex technique using an Elite ABC kit (diluted 1:50, PK-6100; Vector Laboratories, Burlingame, CA, USA). Immunoreactivity was visualized with diaminobenzidine tetrahydrochloride reagent (ImmPACT^{TM} DAB peroxidase substrate kit, SK-410; Vector Laboratories). The immunolabeled sections were counterstained by Mayer’s hematoxylin. For quantitative analyses of immunolabeled sections, the positive area of type II and X collagen in the callus was identified using the color deconvolution plugin in Fiji/ImageJ [39]. Values were normalized to the total callus area.

187

188 *2.6. Cells*

189 MC3T3-E1 mouse osteoblasts were provided by the RIKEN BioResource center (Tokyo,
190 Japan). Cells were routinely maintained on 100-mm dishes coated with type I collagen
191 (Corning, NY, USA) in α-minimum essential medium (α-MEM; Wako Pure Chemical)
192 supplemented with 10% fetal bovine serum (FBS; Gibco, Carlsbad, CA, USA) and 1%
193 penicillin-streptomycin (Wako Pure Chemical) in a humidified 5% CO_2 balanced-air
194 incubator at 37°C. The medium was changed every 3 days.

195 Ocy454-12H murine osteocytes, a clonal derivative of Ocy454 cells that are highly
196 responsive to mechanical forces [41], were provided by the MGH Center for Skeletal
197 Research (Boston, MA, USA). Cells were cultured on collagen-coated dishes in α-MEM
198 (Wako Pure Chemical) containing 10% heat-inactivated FBS (Gibco) and 1% penicillin-
199 streptomycin (Wako Pure Chemical). Ocy454 cells were seeded at 6.0×10^5 cells per 100
200 mm diameter dish (Corning) and grown to the confluence at 33°C, then maintained at 37°C
201 with medium changes every 3 days before 3D co-culture experiments.

202

203 *2.7. 3D osteocyte-osteoblast co-culture*

204 To mimic the *in vivo* environment, Ocy454 osteocytes were three-dimensionally co-cultured
205 with MC3T3-E1 osteoblasts as previously described with some modifications [42]. A type I
206 collagen solution (#5153; Advanced BioMatrix, Carlsbad, CA, USA) was mixed with a
207 neutralizing solution (#5155; Advanced BioMatrix) according to the manufacturer's
208 instructions. The neutralized collagen solution was mixed 1:1 with 2 × α-MEM containing
209 4.4 g/L $NaHCO_3$. Ocy454 cells were added to the collagen solution on the ice at a cell
210 density of 1.5×10^6 cells/mL, and 1 mL was distributed in 12-well plastic plates (Corning)
211 for polymerization at 37°C for 1 hour. MC3T3-E1 cells in 1 mL α-MEM with 10% FBS
212 (Gibco) were then seeded on the surface of each gel (3.0×10^5 cells/well) and incubated at
213 37°C for 48 hours before ultrasound exposure. In some experiments, MC3T3-E1 cells were
214 three-dimensionally cultured without the Ocy454 cells to detect osteocyte functions.

215

216 *2.8. Piezo1 siRNA transfection*

217 The siRNA targeting Piezo1 and negative control were designed and synthesized by Thermo
218 Fisher Scientific (#s107969 and #AM4611; Waltham, MA, USA). Ocy454 cells were seeded
219 in 6-well plates at a density of 2.0×10^5 cells/well 24 hours before the transfection. Cells

were then transfected with control or Piezo1 siRNAs using Lipofectamine RNAi MAX reagent (Thermo Fisher Scientific). After transfection with siRNA for 48 hours, Ocy454 cells were embedded in the collagen gel as described above, and native MC3T3-E1 cells were seeded on the surface of the gel. The transfected cells with the 3D co-culture system were cultured under standard conditions for 48 hours before ultrasound stimulation.

2.9. In vitro ultrasound exposure

The 3D co-cultured cells were exposed to ultrasound through the bottom of the 12-well plate on a clean bench at room temperature. Coupling gel was applied between the probe and the plate, and a piece of sterilized silicone was immersed in the culture medium to absorb ultrasound energy. Cells were exposed to ultrasound using a circular ultrasound transducer with a diameter of 3.3 cm (ULTRASON RE-3000; Nihon Medix), operating at a frequency of 1.5 MHz with a pulse duration of 200 μs and a repetition frequency of 1 kHz. The exposure time was 20 min, and the ultrasound intensity (I_{SATA}) was set to 0.04 or 0.2 W/cm^2. The control plates were exposed to the same conditions as the treated plates without ultrasound. The 3D co-cultured cells were cultured in the 5% CO_2 incubator at 37°C for the indicated times after ultrasound exposure.

2.10. RNA extraction and real-time polymerase chain reaction (PCR)

RNA samples were extracted separately from the surface (MC3T3-E1 osteoblasts) and gel-embedded cells (Ocy454 osteocytes) of co-cultures 1 or 24 hours after ultrasound exposure as previously described [42]. Briefly, gels were first incubated for 60 seconds with 1 mL QIAzol (Qiagen, Hilden, Germany) to collect the surface osteoblasts, and then the underlying gels were dissolved in a separate 1 mL QIAzol aliquot to extract RNA from gel-embedded osteocytes. Total RNA was then extracted from each cell lysis using the RNeasy Mini kit (Qiagen) according to the manufacturer's protocols. The quality of the isolated RNA was checked by measuring the optical density 260/280 using a BioPhotometer D3 (Eppendorf, Hamburg, Germany). Total RNA and TaqMan™ Fast Virus 1-Step Master Mix (Thermo Fisher Scientific) were used for reverse transcription. Real-time PCR reactions were conducted using the Step One Real-Time PCR System (Applied Biosystems, Foster City, CA, USA) with TaqMan gene expression assays (Applied Biosystems) for Runx2 (Mm00501580_m1), Col1a1 (Mm00801666_g1), Alpl (Mm00475834_m1), Bglap3 (Ocn; Mm01741771_g1), Sost (Mm00470479_m1), Dkk1 (Mm00438422_m1), Piezo1

(Mm01241549_m1), and Gapdh (Mm99999915_g1). Gapdh was used as a housekeeping control for calculating the relative expression of each target gene by using the $2^{-\Delta\Delta Ct}$ method.

2.11. Statistical analysis

Statistical analyses were conducted with EZR (Saitama Medical Center, Jichi Medical University, Saitama, Japan), which is a graphical user interface for R (The R Foundation for Statistical Computing, Vienna, Austria) [43]. The results were compared among groups with an unpaired t-test or one-way ANOVA test followed by the Tukey HSD test. Allen's score was compared between groups with a Kruskal-Wallis nonparametric test followed by the Steel-Dwass test. All values are presented here as the median and interquartile range. P values less than 0.05 were considered significant.

3. Results

3.1. Higher-intensity ultrasound than LIPUS accelerated fracture callus mineralization

To investigate the effects of ultrasound exposure at different intensities on osteoporotic fracture healing, mice were treated daily with ultrasound at intensities of 0.04 or 0.2 W/cm^2 (Fig. 1A). μCT analysis showed that ultrasound exposure at 0.2 W/cm^2 increased BMD in the fracture callus on days 14, 21, and 28 post-fracture compared to the untreated mice (Fig. 1B-D and S1A-C). In addition, BMD was higher in the US-0.2 W/cm^2 group than in the US-0.04 W/cm^2 group on day 14 post-fracture. BMD in the US-0.04 W/cm^2 group was statistically similar to that in the control group at all time points. Complete callus bridging was observed in the 0.2 W/cm^2 ultrasound-treated group on day 28 post-fracture, whereas only partial bridging was observed in the untreated group (Fig. S1C). No remarkable changes were observed in BV/TV at the fracture site (Fig. 1E).

The mechanical strength of the fractured femur on day 28 was assessed by the standard three-point bending test. Ultrasound exposure did not affect the maximum load of the fractured femur (Fig. 2A and B). However, the 0.2 W/cm^2-treated femur had a greater displacement to failure (Fig. 2A), and its energy to failure was higher than that of the untreated mice (Fig. 2C).

3.2. Higher-intensity ultrasound than LIPUS accelerated endochondral ossification

To investigate the effects of ultrasound on endochondral ossification, the fracture callus was evaluated histologically by Safranin O/Fast green and alcian blue/picrosirius red staining

(Fig. 3A and S2A). The degree of fracture healing as assessed by the Allen's grading system was greater in the US-0.2 W/cm^2 group than in the control and US-0.04 W/cm^2 groups on day 14 post-fracture (Fig. 3B). Ultrasound exposure did not affect the fracture callus area at any time point (Fig. 3C and S2B). On day 7 post-fracture, more cartilage formation was observed in the ultrasound-exposed femur, but the difference was not significant (Fig. 3D and S2C). Conversely, the cartilage area in the fracture callus of the US-0.2 W/cm^2 group was lower than that of the control or US-0.04 W/cm^2 group on day 14 (Fig. 3D and S2C). Ultrasound exposure at 0.2 W/cm^2 increased new bone formation in the callus on day 14 compared to the untreated and 0.04 W/cm^2-treated mice (Fig. 3E). In Picrosirius red/Alcian blue-stained sections, an increase in new bone mass was observed in the US-0.2 W/cm^2 group not only on day 14 but also on day 7 (Fig. S2D). Fibrous tissue area, tissue other than bone and cartilage in the callus, was less in the US-0.2 W/cm^2 group than in the control group on days 7 and 14 (Fig. S2E).

Type II collagen-positive areas were greater in the 0.2 W/cm^2-treated mice than in the untreated mice on day 7 (Fig. 4A and B). Although few type X collagen-positive cells were observed in the untreated callus on day 7, more positive cells were observed in the 0.2 W/cm^2-treated callus (Fig. 4A). The percentage of type X collagen-positive area in the callus was statistically higher in the US-0.2 W/cm^2 group than in the control and US-0.04 W/cm^2 groups only on day 7 (Fig. 4C). ALP staining revealed that many ALP-positive cells were present in the fracture callus of 0.2 W/cm^2-treated mice on day 7, but few in untreated and 0.04 W/cm^2-treated mice (Fig. 4D and E). In addition, the ALP-positive area on the new bone surface remained greater in the US-0.2 W/cm^2 group than in the control and US-0.04 W/cm^2 groups on day 14 (Fig. 4E). Ultrasound exposure did not affect the osteoclast activity by TRAP staining at any time point (Fig. 4D and F).

3.3. Piezo1 inhibition attenuated fracture callus mineralization after ultrasound exposure

To understand the mechanisms by which higher-intensity ultrasound accelerates fracture healing, we investigated the effects of inhibiting the mechanosensitive ion channel Piezo1 on the fracture healing process (Fig. 5A). Pharmacological inhibition of Piezo1 with GsMTx4 for 2 weeks induced bone loss in the unfractured femur (Fig. S3A-C). Ultrasound exposure at 0.2 W/cm^2 enhanced callus mineralization of vehicle-treated mice on day 14 post-fracture as confirmed by higher BMD, but the difference was not significant (P = 0.077) (Fig. 5B and C). The ultrasound-induced callus mineralization was not observed in GsMTx4-treated mice

(P = 0.771) (Fig. 5C). BV/TV in the callus was not affected by either ultrasound or GsMTx4 treatment (Fig. S3D). Histological score of fracture healing is greater in the ultrasound-treated vehicle mice, but the difference was not significant compared to untreated vehicle mice (P = 0.088) (Fig. 5D and E). The score was comparable between GsMTx4 mice and ultrasound-treated GsMTx4 mice (P = 1.000). Ultrasound or GsMTx4 treatment did not affect callus size and cartilage area on day 14 post-fracture (Fig. 5F, G, and S3E-G). Ultrasound exposure increased newly formed bone in the callus, but GsMTx4 administration attenuated the ultrasound-induced increase (Fig. 5H and S3H). Furthermore, ultrasound increased the ALP-positive area in the callus in vehicle mice, but not in GsMTx4-treated mice (P = 0.501) (Fig. 5I and J). Fibrous area, type II collagen, type X collagen, and TRAP-positive area on day 14 were not altered by either ultrasound or GsMTx4 treatment (Fig. S1I-O).

3.4. Higher-intensity ultrasound increased bone formation-related genes in the 3D osteocyte-osteoblast co-culture system

To gain further insight into the osteogenesis-promoting effects of higher-intensity ultrasound than LIPUS, collagen gel-embedded Ocy454 osteocytes were three-dimensionally co-cultured with MC3T3-E1 osteoblasts and exposed to ultrasound at 0.2 or 0.04 W/cm^2 (Fig. 6A). Sclerostin mRNA expression in osteocytes was comparable between groups 1 hour after ultrasound exposure (Fig. 6B), but its expression was reduced by ultrasound at 0.2 W/cm^2 after 24 hours compared to the untreated cells (Fig. 6D). The expression of Dkk1 in osteocytes is lower in the US-0.2 W/cm^2 group than in the control group 1 hour after ultrasound exposure, but the difference was not significant (P = 0.063) (Fig. 6B). In RNA samples extracted from osteoblasts on the collagen gel surface, ultrasound at 0.2 W/cm^2 increased Runx2, Col1a1, and Alpl expression 1 hour after exposure compared to the untreated cells, but not Ocn (Fig. 6C). The expression of Runx2 and Alpl was also higher in the US-0.2 W/cm^2 group than in the US-0.04 W/cm^2 group. After 24 hours of the exposure, Runx2 and Col1a1 expression levels returned to baseline, whereas Alpl expression remained higher than in the control group (Fig. 6E). Ocn expression showed a non-significant increase in the US-0.2 W/cm^2 group 24 hours after ultrasound exposure (P = 0.061; versus the control group) (Fig. 6E).

3.5. Osteocyte Piezo1 inhibition attenuated bone formation-related gene expression in osteoblasts after ultrasound exposure

To determine the role of osteocytes in ultrasound-induced bone formation, MC3T3-E1 osteoblasts were cultured on the collagen gel with or without Ocy454 osteocytes. Changes in osteoblastic genes after ultrasound exposure were compared with or without osteocytes (Fig. 7A). As a result, ultrasound increased the expression of osteoblastic genes with or without osteocytes, but the expression of Runx2 and Alpl after ultrasound exposure was higher in osteocyte-osteoblast co-culture than in osteoblast single culture (Fig. 7B-E). Next, to investigate whether Piezo1 in osteocytes mediates the ultrasound-induced bone formation, Piezo1 was knocked down in Ocy454 osteocytes by siRNA (Fig. 8A). The siRNA transfection was reduced Piezo1 expression in collagen gel-embedded osteocytes (Fig. 8B). Ultrasound exposure decrease Sost expression in osteocytes, but the difference was not significant ($P = 0.094$) (Fig. 8C). The expression of Sost was comparable between untreated cells and ultrasound-treated cells in Piezo1 knockdown osteocytes ($P = 0.994$). Ultrasound decreased Dkk1 expression to a similar extent in both control and Piezo1 siRNA-transfected osteocytes (Fig. 8D). Ultrasound exposure increased Runx2 expression in osteoblasts, whereas the difference was not detected when osteoblasts were co-cultured with Piezo1 knockdown osteocytes ($P = 0.259$) (Fig. 8E). There was no apparent difference in Col1a1 expression in osteoblasts (Fig. 8F). The expression of Alpl was increased by ultrasound exposure in with or without Piezo1 siRNA, whereas its expression was lower in the Piezo1 siRNA cells than in the control siRNA cells (Fig. 8G). Ocn expression in osteoblasts was increased by ultrasound exposure regardless of the presence or absence of Piezo1 in osteocytes (Fig. 8H).

4. Discussion

This study explored the effects of different ultrasound intensities on fracture healing. Our findings showed that higher-intensity ultrasound than LIPUS increased cartilage formation and osteoblastic activity in the fracture callus, thereby accelerating endochondral ossification in the early stages of fracture healing. In addition, the inhibition of Piezo1 *in vivo* and *in vitro* attenuated fracture callus mineralization and bone formation after ultrasound exposure, suggesting that Piezo1-mediated mechanotransduction is involved, at least in part, in ultrasound-induced acceleration of fracture healing.

The early stages of fracture healing are characterized by chondrogenesis. The chondrogenic area was observed in the fracture callus on day 7 post-fracture, and ultrasound at an intensity of 0.2 W/cm^2 increased the type II collagen-positive area in the callus. Although several reports have shown increased chondrogenesis in the fracture callus after LIPUS exposure [44,45], our results indicate that higher-intensity ultrasound than LIPUS can promote chondrogenesis in the early stages of fracture. This is consistent with some previous results, which have observed that ultrasound promotes chondrogenic differentiation of mesenchymal stem cells in an intensity-dependent manner [15,16]. The chondrogenic area in the callus is determined by the magnitude of local strain and hydrostatic pressure, and greater mechanical stress at fracture sites promotes chondrogenic differentiation of mesenchymal stem cells [46]. In light of these findings, higher-intensity ultrasound may produce greater mechanical stress at the fracture site than LIPUS, resulting in more chondrogenesis in the early stages of fracture. Hypertrophic chondrocytes differentiate from mature chondrocytes in the callus, which mediates the cartilage-to-bone transition during endochondral ossification [47]. In this study, ultrasound at 0.2 W/cm^2 increased type X collagen-positive cells, a marker of hypertrophic chondrocytes, indicating that higher-intensity ultrasound accelerates the cartilage-to-bone transition. Ultrasound-induced differentiation of hypertrophic chondrocytes is controversial with one report indicating that LIPUS decreases type X collagen in chondrocytes [48], while another study found an increase in cartilage explants [49]. The expression of type X collagen in chondrocytes after ultrasound exposure depends on the ultrasound intensity and cell differentiation stage [50]. Furthermore, ultrasound can stimulate hypertrophy in chondrocytes developing toward terminal differentiation, similar to those in the fracture callus, but not stable hyaline cartilage [49]. Our results indicate that higher-intensity ultrasound may enhance bone formation by increasing the hypertrophy of chondrocytes in the fracture callus. Considered together, our results suggest that higher-intensity ultrasound than LIPUS stimulates cartilage formation and hypertrophic differentiation of chondrocytes in the early stages of fracture, resulting in accelerated endochondral ossification.

Besides cartilage formation, higher-intensity ultrasound than LIPUS enhanced osteoblastic differentiation in the fracture callus as reflected by an increased ALP-positive area. In support of this, ultrasound-intensity dependent effects on osteoblastic activation were observed in the bone defect [12,51] and ovariectomy-induced osteoporosis models [13,14]. Our results also show that higher-intensity ultrasound, but not LIPUS, enhances

osteoblastic activity in a transverse fracture model that develops through endochondral ossification similar to human fractures. Osteoblasts in the fracture callus have long been thought to be provided by the progenitor cells that enter the callus with vascularization following the hypertrophic chondrocyte apoptosis [52]. However, accumulating evidence suggests that hypertrophic chondrocytes are a major source of osteoblasts in the callus and that transdifferentiation of chondrocytes into osteoblasts is the dominant pathway for endochondral ossification during fracture healing [53]. In the present study, ultrasound exposure increased hypertrophic chondrocytes in the callus, which may lead to increased osteoblasts and ultimately accelerated callus mineralization. Further research is needed to determine whether mechanical stress, such as ultrasound, can stimulate the transdifferentiation of hypertrophic chondrocytes into osteoblasts. Osteoclasts labeled with TRAP, the main cells involved in callus remodeling, were not affected by ultrasound exposure in this study. The effects of ultrasound on osteoclasts are controversial with studies showing increased [54], decreased [55], or no change [12] in osteoclast activity *in vivo* and *in vitro*. Moreover, knockout mice for cathepsin K, a major substrate protein of osteoclasts, accelerate callus mineralization due to increased osteoblastic bone formation without osteoclast changes [56]. In summary, higher-intensity ultrasound than LIPUS accelerates fracture healing by increasing osteoblastic bone formation in the callus, but not osteoclastic callus resorption.

For ultrasound to have a biological effect, the mechanical signals must be converted into biochemical signals inside the cells. Piezo1 channel is activated by mechanical stress in bone cells and is involved in physiological processes in bone via intracellular calcium signaling [24–26]. In this study, ultrasound-stimulated fracture callus mineralization and new bone formation were suppressed by Piezo1 inhibition through GsMTx4 administration. Several *in vitro* studies have shown that ultrasound acoustic waves activate Piezo1 in various cell types [27–30], and our results suggest that Piezo1 is also essential for ultrasound sensing *in vivo*. Piezo1 is also expressed in chondrocytes and contributes to endochondral ossification in the growth plate [57], and administration of Yoda1, a Piezo1 agonist, accelerates fracture healing [31], indicating that activation of Piezo1 may accelerate endochondral ossification. These results indicate that the Piezo1 channel may transduce ultrasonic mechanical signals into biochemical signals *in vivo*, which plays a critical role in ultrasound-stimulated fracture healing. Unexpectedly, in contrast to previous studies reporting that genetic inhibition of Piezo1 delayed fracture healing [31,32], administration of

GsMTx4 did not affect normal fracture healing. Unlike genetic approaches, pharmacological inhibition using GsMTx4 may affect ion channels other than Piezo1, such as the activation of TREK-1, which is responsible for mechanotransduction sensing in osteoblasts [58,59]. Given the complex mechanical-biological interactions in the fracture healing process, different approaches to Piezo1 inhibition may lead to different outcomes in fracture healing. The role of Piezo1 in normal fracture healing is only partially understood and requires further investigation.

Osteocytes play an important role in mechanotransduction in bone and also in the fracture healing process [21]. To elucidate the role of osteocytes in ultrasound-stimulated bone formation, we developed a 3D osteocyte-osteoblast co-culture system to investigate the effects of ultrasound on mechanotransduction between osteocytes and osteoblasts. The results showed that higher-intensity ultrasound than LIPUS downregulated sclerostin expression in osteocytes and upregulated bone formation-related gene expression in osteoblasts. The mechanosensitive protein sclerostin negatively regulates osteoblastic bone formation via canonical Wnt signaling [60]. Dkk1, an another strong Wnt antagonist [61], also showed a non-significant decrease after ultrasound exposure. Thus, ultrasound may promote bone formation in osteoblasts by decreasing Wnt antagonist gene expression in osteocytes. Nonetheless, ultrasound at LIPUS intensity did not affect the expression of sclerostin, Dkk1, and bone formation-related genes. This is consistent with our previous *in vivo* study showing that higher-intensity ultrasound decreases sclerostin expression in cortical bone, but not LIPUS intensity [12]. These findings support that sclerostin expression is downregulated in mechanical stress magnitude-dependent manner [60], suggesting that only higher-intensity ultrasound induces mechanotransduction in osteocytes, leading to enhanced osteoblastic bone formation. The expression of Runx2 and Alpl after ultrasound exposure was lower in the osteoblast single culture than in the osteocyte-osteoblast co-culture in this study. This result suggests that osteocytes play a role in ultrasound-induced osteoblastic bone formation. Previous studies have also shown the importance of osteocytes in ultrasound responses, reporting that conditioned media from ultrasound-stimulated osteocytes promotes osteoblast differentiation [22]. Additionally, ultrasound does not affect fracture healing in medaka, whose bones lack osteocytes [23]. Furthermore, the ultrasound-induced downregulation of sclerostin in osteocytes was attenuated by osteocytic Piezo1 knockdown in osteocyte-osteoblast co-culture. Sclerostin is known to be downstream of the Piezo1-Akt signaling pathway in osteocytes [62]. In contrast, the expression of osteocytic

Dkk1 after ultrasound was not altered by Piezo1 knockdown. While Dkk1 has been indirectly suggested to be a downstream target of Piezo1 [63], our *in vitro* knockdown experiments indicate that Piezo1 may not be involved in the ultrasound-induced decrease in osteocytic Dkk1 expression. Thus, our results suggest that osteocytic Piezo1 is activated by ultrasound acoustic waves and induces mechanotransduction via sclerostin downregulation. Osteocytic Piezo1 knockdown affected not only osteocytes but also osteoblasts, attenuating ultrasound-induced osteoblastic gene (Runx2 and Alpl) expression. Runx2 and Alpl are activated by canonical Wnt signaling in osteoblasts, which is negatively regulated by osteocytic sclerostin [64,65]. Therefore, osteocytic Piezo1 may mediate ultrasound-stimulated osteoblastic bone formation through mechanotransduction between osteocytes and osteoblasts via sclerostin regulation. Collectively, these findings suggest that osteocytes are essential for ultrasound-induced bone formation and that osteocytic Piezo1 is involved in ultrasound sensing and response.

This study has several potential limitations. First, we used a rodent fracture model to investigate the effects of different ultrasound intensities. Soft tissues in humans are thicker than in mice, and therefore it remains unclear whether an ultrasound intensity of 0.2 W/cm^2 is optimal for human fractures due to the attenuation effect of ultrasound. However, when the ultrasound pressure field is considered, the acoustic pressure on the bone is comparable between ultrasound applied to rodent limbs and human femurs, the deepest clinically treated bone [19]. The stages of fracture healing in mice match those observed clinically, and many studies have reported the therapeutic effects of ultrasound using rodent models [45,66,67]. Second, our study investigated the effects of Piezo1-mediated mechanotransduction using male mice. The estrogen status in bone has been shown to affect bone mechanotransduction [34,68]. Understanding sex differences in the relationship between ultrasound and bone mechanotransduction is important for the therapeutic strategies of postmenopausal osteoporotic fractures. Finally, this study demonstrated the role of Piezo1 in ultrasound-stimulated fracture healing using the Piezo1 inhibitor GsMTx4, but was unable to elucidate even cell type-specific Piezo1 function. Although our *in vitro* results showed that osteocytic Piezo1 is involved in ultrasound-stimulated bone formation, Piezo1 in periosteal stem cells and endothelial cells have been reported to contribute to fracture healing [31,32]. In addition, GsMTx4 is known to affect ion channels other than Piezo1 [58], and its off-target effects should be noted. Further studies are needed to better define the mechanism by which Piezo1

contributes to ultrasound-stimulated fracture healing using calcium imaging and cell type-specific knockout mice.

5. Conclusion

In conclusion, this study demonstrates that higher-intensity ultrasound than clinically used LIPUS can accelerate endochondral ossification after fracture by promoting chondrogenesis and osteoblast differentiation in the fracture callus. Furthermore, our results suggest that mechanotransduction via Piezo1 mediates, at least in part, ultrasound-stimulated fracture healing and bone formation. The ultrasound intensity of 0.2 W/cm^2 in this study is within the range of non-invasive intensities used clinically for pain and soft tissue injury [69]. Ultimately, this modality needs to be scaled up to humans before its clinical utility can be realized; however, we provide a potential novel mechanobiological approach for accelerating fracture healing.

CRediT authorship contribution statement

Shota Inoue: Conceptualization, Methodology, Formal analysis, Investigation, Funding acquisition, Writing - Original Draft. **Changxin Li:** Investigation, Writing – review & editing. **Junpei Hatakeyama:** Investigation, Writing – review & editing. **Hanlin Jiang:** Investigation, Writing – review & editing. **Hiroshi Kuroki:** Resources, Writing – review & editing. **Hideki Moriyama:** Conceptualization, Methodology, Resources, Data Curation, Supervision, Funding acquisition, Writing - Review & Editing.

Conflict of interest

The authors have no conflict of interest to declare.

Data availability

The data that support the findings of this study are available from the corresponding author upon reasonable request.

Funding

This work was supported by a Research Fellowship of the Japan Society for the Promotion of Science for Young Scientists (21J13006) and the Japan Society for the Promotion of Science KAKENHI Grant (16K12933).

Acknowledgments

We thank Mr. Yoshio Wakimoto, Mr. Bin Liu, Mr. Daisuke Eguchi, Mr. Masahiro Wakayama, and Mr. Ryo Yokoi for their skilled technical assistance; Assoc. Prof. Noriaki Maeshige and Mr. Atomu Yamaguchi for their support with cell culture technique; and Assoc. Prof. Akira Ito and Mr. Hideki Kawai for their support with mechanical testing.

References

[1] T.A. Einhorn, L.C. Gerstenfeld, Fracture healing: mechanisms and interventions, Nat. Rev. Rheumatol. 11 (2015) 45–54.

[2] O. Johnell, J.A. Kanis, An estimate of the worldwide prevalence, mortality and disability associated with hip fracture, Osteoporos. Int. 15 (2004) 897–902.

[3] R.S. Braithwaite, N.F. Col, J.B. Wong, Estimating hip fracture morbidity, mortality and costs, J. Am. Geriatr. Soc. 51 (2003) 364–370.

[4] J.D. Heckman, J.P. Ryaby, J. McCabe, J.J. Frey, R.F. Kilcoyne, Acceleration of tibial fracture-healing by non-invasive, low-intensity pulsed ultrasound, J. Bone Joint. Surg. Am. 76 (1994) 26–34.

[5] T.K. Kristiansen, J.P. Ryaby, J. McCabe, J.J. Frey, L.R. Roe, Accelerated healing of distal radial fractures with the use of specific, low-intensity ultrasound: A multicenter, prospective, randomized, double- blind, placebo-controlled study, J. Bone Joint. Surg. Am. 79 (1997) 961–973.

[6] J.W. Busse, M. Bhandari, T.A. Einhorn, E. Schemitsch, J.D. Heckman, P. Tornetta, K.S. Leung, D. Heels-Ansdell, S. Makosso-Kallyth, G.J. Della Rocca, C.B. Jones, G.H. Guyatt, Re-evaluation of low intensity pulsed ultrasound in treatment of tibial fractures (TRUST): Randomized clinical trial, BMJ. 355 (2016). https://doi.org/10.1136/bmj.i5351.

[7] S. Schandelmaier, A. Kaushal, L. Lytvyn, D. Heels-Ansdell, R.A.C. Siemieniuk, K.A. Aguiar, G.H. Guyatt, P.O. Vandvik, R. Couban, B. Mollon, J.W. Busse, Low intensity pulsed ultrasound for bone healing: systematic review of randomized controlled trials, BMJ. 356 (2017) j656.

[8] L. Handolin, V. Kiljunen, I. Arnala, M.J. Kiuru, J. Pajarinen, E.K. Partio, P. Rokkanen, Effect of ultrasound therapy on bone healing of lateral malleolar fractures of the ankle joint fixed with bioabsorbable screws, J. Orthop. Sci. 10 (2005) 391–395.

[9] A. Emami, M. Petrén-Mallmin, S. Larsson, No effect of low-intensity ultrasound on healing time of intramedullary fixed tibial fractures, J. Orthop. Trauma. 13 (1999) 252–257.

[10] E. Fávaro-Pípi, S.M. Feitosa, D.A. Ribeiro, P. Bossini, P. Oliveira, N.A. Parizotto, A.C.M. Renno, Comparative study of the effects of low-intensity pulsed ultrasound and low-level laser therapy on bone defects in tibias of rats, Lasers Med. Sci. 25 (2010) 727–732.

[11] A.J. Fontes-Pereira, M. Amorim, F. Catelani, D.P. Matusin, P. Rosa, D.M. Guimarães, M.A. von Krüger, W.C. de A. Pereira, The influence of low-intensity physiotherapeutic ultrasound on the initial stage of bone healing in rats: an experimental and simulation study, J. Ther. Ultrasound. 4 (2016) 24.

[12] S. Inoue, J. Hatakeyama, H. Aoki, H. Kuroki, T. Niikura, K. Oe, T. Fukui, R. Kuroda, T. Akisue, H. Moriyama, Effects of ultrasound, radial extracorporeal shock waves, and electrical stimulation on rat bone defect healing, Ann. N. Y. Acad. Sci. (2021) nyas.14581.

[13] S. Sun, L. Sun, Y. Kang, L. Tang, Y.X. Qin, D. Ta, Therapeutic effects of low-intensity pulsed ultrasound on osteoporosis in ovariectomized rats: intensity-dependent study, Ultrasound Med. Biol. 46 (2020) 108–121.

[14] S. Inoue, J. Hatakeyama, H. Aoki, H. Kuroki, T. Niikura, K. Oe, T. Fukui, R. Kuroda, T. Akisue, H. Moriyama, Utilization of mechanical stress to treat osteoporosis: the effects of electrical stimulation, radial extracorporeal shock wave, and ultrasound on experimental osteoporosis in ovariectomized rats, Calcif. Tissue Int. 109 (2021). 215-229.

[15] J. Wang, N. Tang, Q. Xiao, L. Zhao, Y. Li, J. Li, J. Wang, Z. Zhao, L. Tan, The potential application of pulsed ultrasound on bone defect repair via developmental engineering: an in vitro study, Artif. Organs. 40 (2016) 505–513.

[16] X. Wang, Q. Lin, T. Zhang, X. Wang, K. Cheng, M. Gao, P. Xia, X. Li, Low-intensity pulsed ultrasound promotes chondrogenesis of mesenchymal stem cells via regulation of autophagy, Stem Cell Res. Ther. 10 (2019) 41.

[17] K. Sena, S.R. Angle, A. Kanaji, C. Aher, D.G. Karwo, D.R. Sumner, A.S. Virdi, Low-intensity pulsed ultrasound (LIPUS) and cell-to-cell communication in bone marrow stromal cells, Ultrasonics. 51 (2011) 639–644.

[18] C.H. Tang, R.S. Yang, T.H. Huang, D.Y. Lu, W.J. Chuang, T.F. Huang, W.M. Fu, Ultrasound stimulates cyclooxygenase-2 expression and increases bone formation through integrin, focal adhesion kinase, phosphatidylinositol 3-kinase, and Akt pathway in osteoblasts, Mol. Pharmacol. 69 (2006) 2047–2057.

[19] A. Harrison, S. Lin, N. Pounder, Y. Mikuni-Takagaki, Mode & mechanism of low intensity pulsed ultrasound (LIPUS) in fracture repair, Ultrasonics. 70 (2016) 45–52.

[20] F.G.F. Tresguerres, J. Torres, J. López-Quiles, G. Hernández, J.A. Vega, I.F. Tresguerres, The osteocyte: A multifunctional cell within the bone, Ann. Anat. 227 (2020) 151422.

[21] M.H.V. Choy, R.M.Y. Wong, S.K.H. Chow, M.C. Li, Y.N. Chim, T.K. Li, W.T. Ho, J.C.Y. Cheng, W.H. Cheung, How much do we know about the role of osteocytes in different phases of fracture healing? A systematic review, J. Orthop. Translat. 21 (2020) 111–121.

[22] L. Li, Z. Yang, H. Zhang, W. Chen, M. Chen, Z. Zhu, Low-intensity pulsed ultrasound regulates proliferation and differentiation of osteoblasts through osteocytes, Biochem. Biophys. Res. Commun. 418 (2012) 296–300.

[23] T. Shimizu, N. Fujita, K. Tsuji-Tamura, Y. Kitagawa, T. Fujisawa, M. Tamura, M. Sato, Osteocytes as main responders to low-intensity pulsed ultrasound treatment during fracture healing, Sci. Rep. 11 (2021) 10298.

[24] L. Wang, X. You, S. Lotinun, L. Zhang, N. Wu, W. Zou, Mechanical sensing protein PIEZO1 regulates bone homeostasis via osteoblast-osteoclast crosstalk, Nat. Commun. 11 (2020) 1–12.

[25] W. Sun, S. Chi, Y. Li, S. Ling, Y. Tan, Y. Xu, F. Jiang, J. Li, C. Liu, G. Zhong, D. Cao, X. Jin, D. Zhao, X. Gao, Z. Liu, B. Xiao, Y. Li, The mechanosensitive Piezo1 channel is required for bone formation, Elife. 8 (2019) e47454.

[26] X. Li, L. Han, I. Nookaew, E. Mannen, M.J. Silva, M. Almeida, J. Xiong, Stimulation of Piezo1 by mechanical signals promotes bone anabolism, Elife. 8 (2019) e49631.

[27] L. Zhang, X. Liu, L. Gao, Y. Ji, L. Wang, C. Zhang, L. Dai, J. Liu, Z. Ji, Activation of Piezo1 by ultrasonic stimulation and its effect on the permeability of human umbilical vein endothelial cells, Biomed. Pharmacother. 131 (2020) 110796.

[28] Z. Qiu, J. Guo, S. Kala, J. Zhu, Q. Xian, W. Qiu, G. Li, T. Zhu, L. Meng, R. Zhang, H.C. Chan, H. Zheng, L. Sun, The mechanosensitive ion channel piezo1 significantly mediates in vitro ultrasonic stimulation of neurons, IScience. 21 (2019) 448–457.

[29] Q. Gao, P.R. Cooper, A.D. Walmsley, B.A. Scheven, Role of piezo channels in ultrasound-stimulated dental stem cells, J. Endod. 43 (2017) 1130–1136.

[30] G. Zhang, X. Li, L. Wu, Y.-X. Qin, Piezo1 channel activation in response to mechanobiological acoustic radiation force in osteoblastic cells, Bone Res. 9 (2021) 16.

[31] Y. Liu, H. Tian, Y. Hu, Y. Cao, H. Song, S. Lan, Z. Dai, W. Chen, Y. Zhang, Z. Shao, Y. Liu, W. Tong, Mechanosensitive Piezo1 is crucial for periosteal stem cell-mediated fracture healing, Int. J. Biol. Sci. 18 (2022) 3961–3980.

[32] P. Chen, G. Zhang, S. Jiang, Y. Ning, B. Deng, X. Pan, S. Liu, Y. He, L. Zhang, R. Wan, Z. Wu, Q. He, J. Yin, H. Wang, J. Li, Mechanosensitive Piezo1 in endothelial cells promotes angiogenesis to support bone fracture repair, Cell Calcium. 97 (2021) 102431.

[33] M.B. Manigrasso, J.P. O'Connor, Characterization of a closed femur fracture model in mice, J. Orthop. Trauma. 18 (2004) 687–695.

[34] L. Steppe, B.T. Krüger, M.E.A. Tschaffon, V. Fischer, J. Tuckermann, A. Ignatius, M. Haffner-Luntzer, Estrogen receptor α signaling in osteoblasts is required for mechanotransduction in bone fracture healing, Front. Bioeng. Biotechnol. 9 (2021) 782355.

[35] K.R. O'Neill, C.M. Stutz, N.A. Mignemi, M.C. Burns, M.R. Murry, J.S. Nyman, J.G. Schoenecker, Micro-computed tomography assessment of the progression of fracture healing in mice, Bone. 50 (2012) 1357–1367.

[36] T. Kawamoto, Use of a new adhesive film for the preparation of multi-purpose fresh-frozen sections from hard tissues, whole-animals, insects and plants, Arch. Histol. Cytol. 66 (2003) 123–143.

[37] L. Montes-Medina, A. Hernández-Fernández, A. Gutiérrez-Rivera, P. Ripalda-Cemboráin, N. Bitarte, V. Pérez-López, F. Granero-Moltó, F. Prosper, A. Izeta, Effect of bone marrow stromal cells in combination with biomaterials in early phases of distraction osteogenesis: An experimental study in a rabbit femur model, Injury. 49 (2018) 1979–1986.

[38] H.L. Allen, A. Wase, W.T. Bear, Indomethacin and aspirin: Effect of nonsteroidal anti-inflammatory agents on the rate of fracture repair in the rat, Acta Orthop. 51 (1980) 595–600.

[39] A.C. Ruifrok, D.A. Johnston, Quantification of histochemical staining by color deconvolution, Anal. Quant. Cytol. Histol. 23 (2001) 291–299.

[40] H. Moriyama, N. Kanemura, I. Brouns, I. Pintelon, D. Adriaensen, J.P. Timmermans, J. Ozawa, N. Kito, T. Gomi, M. Deie, Effects of aging and exercise training on the histological and mechanical properties of articular structures in knee joints of male rat, Biogerontology. 13 (2012) 369–381.

[41] C. Shi, Y. Uda, C. Dedic, E. Azab, N. Sun, A.I. Hussein, C.A. Petty, K. Fulzele, M.C. Mitterberger-Vogt, W. Zwerschke, R. Pereira, K. Wang, P.D. Pajevic, Carbonic anhydrase III protects osteocytes from oxidative stress, FASEB J. 32 (2018) 440–452.

[42] M. Vazquez, B.A.J. Evans, D. Riccardi, S.L. Evans, J.R. Ralphs, C.M. Dillingham, D.J. Mason, A new method to investigate how mechanical loading of osteocytes controls osteoblasts, Front. Endocrinol. 5 (2014) 208.

[43] Y. Kanda, Investigation of the freely available easy-to-use software "EZR" for medical statistics, Bone Marrow Transplant. 48 (2013) 452–458.

[44] M. Coords, E. Breitbart, D. Paglia, N. Kappy, A. Gandhi, J. Cottrell, N. Cedeno, N. Pounder, J.P. O'Connor, S.S. Lin, The effects of low-intensity pulsed ultrasound upon diabetic fracture healing, J. Orthop. Res. 29 (2011) 181–188.

[45] Y. Azuma, M. Ito, Y. Harada, H. Takagi, T. Ohta, S. Jingushi, Low-intensity pulsed ultrasound accelerates rat femoral fracture healing by acting on the various cellular reactions in the fracture callus, J. Bone Miner. Res. 16 (2001) 671–680.

[46] L.E. Claes, C.A. Heigele, Magnitudes of local stress and strain along bony surfaces predict the course and type of fracture healing, J. Biomech. 32 (1999) 255‑266.

[47] J. Kodama, K.J. Wilkinson, M. Iwamoto, S. Otsuru, M. Enomoto-Iwamoto, The role of hypertrophic chondrocytes in regulation of the cartilage-to-bone transition in fracture healing, Bone Rep. 17 (2022) 101616.

[48] S. Mukai, H. Ito, Y. Nakagawa, H. Akiyama, M. Miyamoto, T. Nakamura, Transforming growth factor-beta1 mediates the effects of low-intensity pulsed ultrasound in chondrocytes, Ultrasound Med. Biol. 31 (2005) 1713–1721.

[49] Z.I.-J. Zhang, J. Huckle, C.A. Francomano, R.G.S. Spencer, The influence of pulsed low-intensity ultrasound on matrix production of chondrocytes at different stages of differentiation: an explant study, Ultrasound Med. Biol. 28 (2002) 1547–1553.

[50] Z.J. Zhang, J. Huckle, C.A. Francomano, R.G.S. Spencer, The effects of pulsed low-intensity ultrasound on chondrocyte viability, proliferation, gene expression and matrix production, Ultrasound Med. Biol. 29 (2003) 1645–1651.

[51] B. Lavandier, A. Gleizal, J.C. Béra, Experimental assessment of calvarial bone defect re-ossification stimulation using low-intensity pulsed ultrasound, Ultrasound Med. Biol. 35 (2009) 585–594.

[52] H.M. Kronenberg, Developmental regulation of the growth plate, Nature. 423 (2003) 332–336.

[53] D.P. Hu, F. Ferro, F. Yang, A.J. Taylor, W. Chang, T. Miclau, R.S. Marcucio, C.S. Bahney, Cartilage to bone transformation during fracture healing is coordinated by the invading vasculature and induction of the core pluripotency genes, Development. 144 (2017) 221–234.

[54] M.F.N. Feres, C. Kucharski, S. Diar-Bakirly, T. El-Bialy, Effect of low-intensity pulsed ultrasound on the activity of osteoclasts: An in vitro study, Arch. Oral Biol. 70 (2016) 73–78.

[55] J. Meng, J. Hong, C. Zhao, C. Zhou, B. Hu, Y. Yang, G. Jiang, S. Li, Z. Shi, X. Cai, S. Yan, Low-intensity pulsed ultrasound inhibits RANKL-induced osteoclast formation via modulating ERK-c-Fos-NFATc1 signaling cascades, Am. J. Transl. Res. 10 (2018) 2901–2910.

[56] M.A. Gentile, D.Y. Soung, C. Horrell, R. Samadfam, H. Drissi, L.T. Duong, Increased fracture callus mineralization and strength in cathepsin K knockout mice, Bone. 66 (2014) 72–81.

[57] G. Hendrickx, V. Fischer, A. Liedert, S. von Kroge, M. Haffner-Luntzer, L. Brylka, E. Pawlus, M. Schweizer, T. Yorgan, A. Baranowsky, T. Rolvien, M. Neven, U. Schumacher, D.J. Beech, M. Amling, A. Ignatius, T. Schinke, Piezo1 Inactivation in Chondrocytes Impairs Trabecular Bone Formation, J. Bone Miner. Res. 36 (2021) 369–384.

[58] R. Gnanasambandam, C. Ghatak, A. Yasmann, K. Nishizawa, F. Sachs, A.S. Ladokhin, S.I. Sukharev, T.M. Suchyna, GsMTx4: Mechanism of inhibiting mechanosensitive ion channels, Biophys. J. 112 (2017) 31–45.

[59] S. Hughes, J. Magnay, M. Foreman, S.J. Publicover, J.P. Dobson, A.J. El Haj, Expression of the mechanosensitive 2PK+ channel TREK-1 in human osteoblasts, J. Cell. Physiol. 206 (2006) 738–748.

[60] G.L. Galea, L.E. Lanyon, J.S. Price, Sclerostin's role in bone's adaptive response to mechanical loading, Bone. 96 (2017) 38–44.

[61] D. Schupbach, M. Comeau-Gauthier, E. Harvey, G. Merle, Wnt modulation in bone healing, Bone. 138 (2020) 115491.

[62] F. Sasaki, M. Hayashi, Y. Mouri, S. Nakamura, T. Adachi, T. Nakashima, Mechanotransduction via the Piezo1-Akt pathway underlies Sost suppression in osteocytes, Biochem. Biophys. Res. Commun. 521 (2020) 806–813.

[63] R.-W. Wu, W.-S. Lian, Y.-S. Chen, J.-Y. Ko, S.-Y. Wang, H. Jahr, F.-S. Wang, Piezoelectric Microvibration Mitigates Estrogen Loss-Induced Osteoporosis and Promotes Piezo1, MicroRNA-29a, and Wnt3a Signaling in Osteoblasts, Int. J. Mol. Sci. 22 (2021) 9476.

[64] T. Gaur, C.J. Lengner, H. Hovhannisyan, R.A. Bhat, P.V.N. Bodine, B.S. Komm, A. Javed, A.J. van Wijnen, J.L. Stein, G.S. Stein, J.B. Lian, Canonical WNT signaling promotes osteogenesis by directly stimulating Runx2 gene expression, J. Biol. Chem. 280 (2005) 33132–33140.

[65] E. Matsuzaki, F. Takahashi-Yanaga, Y. Miwa, M. Hirata, Y. Watanabe, N. Sato, S. Morimoto, T. Hirofuji, K. Maeda, T. Sasaguri, Differentiation-inducing factor-1 alters canonical Wnt signaling and suppresses alkaline phosphatase expression in osteoblast-like cell lines, J. Bone Miner. Res. 21 (2006) 1307–1316.

[66] S. J Wang, D.G. Lewallen, M.E. Bolander, E.Y.S. Chao, D.M. Ilstrup, J.F. Greenleaf, Low intensity ultrasound treatment increases strength in a rat femoral fracture model, J. Orthop. Res. 12 (1994) 40–47.

[67] W.-H. Cheung, W.-C. Chin, L. Qin, K.-S. Leung, Low intensity pulsed ultrasound enhances fracture healing in both ovariectomy-induced osteoporotic and age-matched normal bones, J. Orthop. Res. 30 (2012) 129–136.

[68] M. Zhang, F.-M. Chen, A.-H. Wang, Y.-J. Chen, X. Lv, S. Wu, R.-N. Zhao, Estrogen and its receptor enhance mechanobiological effects in compressed bone mesenchymal stem cells, Cells Tissues Organs. 195 (2012) 400–413.

[69] V.J. Robertson, Dosage and treatment response in randomized clinical trials of therapeutic ultrasound, Phys. Ther. Sport. 3 (2002) 124–133.

Figure legends

Fig. 1

Higher-intensity ultrasound than LIPUS accelerated callus mineralization of osteoporotic fracture. (A) Female mice underwent bilateral ovariectomy. Four weeks after the ovariectomy, a standard transverse mid-shaft femoral fracture was created. Mice received ultrasound at intensities of 0.04 or 0.2 W/cm^2 for 20 min/day, 7 days/week starting from day 1 after the fracture. (B) Representative 3D images of fractured femurs are shown. Scale bar = 3 mm. (C) Representative transverse and sagittal μCT images of fractured femurs on day 14 post-fracture are shown. The graphs show (D) bone mineral density (BMD) and (E) bone volume fraction (BV/TV) in the fracture callus. Data are presented as the median and interquartile range. n = 7-8 mice/group/time point.

Fig. 2

Higher-intensity ultrasound than LIPUS promotes recovery of mechanical strength in fractured femurs. (A) Representative load-displacement curves obtained from a three-point bending test are shown. The graphs show (B) maximum load and (C) energy to failure calculated from the load-displacement curves. Data are presented as the median and interquartile range. n = 7-8 mice/group/time point.

Fig. 3

Higher-intensity ultrasound than LIPUS accelerated endochondral ossification of osteoporotic fracture. (A) Representative Safranin-O-stained images of fractured femurs are shown. Scale bar = 500 μm. The graphs show (B) the degree of fracture healing according to Allen's grading system, (C) the fracture callus area and the percentage of (D) cartilage, and (E) the newly formed bone area in the fracture callus. Data are presented as the median and interquartile range. n = 7-8 mice/group/time point.

Fig. 4

Higher-intensity ultrasound than LIPUS stimulated cartilage formation and osteoblast differentiation in the fracture callus. (A) Representative immunostained images for type II collagen and type X collagen of fractured femurs are shown. Scale bar = 100 μm. The graphs show the percentage of (B) type II collagen- and (C) type X collagen-positive area in the

fracture callus. (D) Representative ALP- and TRAP-stained images of fractured femurs are shown. Scale bars = 100 μm. The graphs show the percentage of (E) ALP- and (F) TRAP-positive areas in the fracture callus. Data are presented as the median and interquartile range. n = 7-8 mice/group/time point.

Fig. 5

The Piezo1 inhibitor GsMTx4 attenuated callus mineralization after ultrasound exposure. (A) Male mice underwent mid-shaft femoral fracture. Mice were intraperitoneally injected with vehicle control (saline) or 1 mg/kg GsMTx4 every day. The mice were exposed to the ultrasound at an intensity of 0.2 W/cm^2 for 20 min/day, 7 days/week. Fractured femurs were collected 14 days after the fracture. (B) Representative 3D images of fractured femurs are shown. Scale bar = 3 mm. (C) The graph shows the bone mineral density (BMD) in the fracture callus. (D) Representative Safranin-O-stained images of fractured femurs are shown. Scale bar = 500 μm. The graphs show (E) the degree of fracture healing as assessed by Allen's grading system, (F) the fracture callus area, and the percentage of (G) cartilage, and (H) the newly formed bone area in the fracture callus. (I) Representative ALP-stained images of fractured femurs are shown. Scale bars = 100 μm. (E) The graphs show the percentage of ALP-positive area in the fracture callus. Data are presented as the median and interquartile range. n = 5-6 mice/group.

Fig. 6

Higher-intensity ultrasound than LIPUS increased bone formation-related genes in 3D osteocyte-osteoblast co-culture. (A) Ocy454 osteocytes were three-dimensionally co-cultured with MC3T3-E1 osteoblasts. The 3D co-cultured cells were exposed to ultrasound at intensities of 0.04 or 0.2 W/cm^2 for 20 min. RNA samples were extracted separately from the surface (MC3T3-E1 osteoblasts) and gel-embedded cells (Ocy454 osteocytes) 1 or 24 h after ultrasound exposure. The graphs show the mRNA expression of Sost and Dkk1 in osteocytes and Runx2, Col1a1, Alpl, and Ocn in osteoblasts (B and C) 1 hour or (D and E) 24 hours after ultrasound exposure. Data are presented as the median and interquartile range. n = 4 per group.

Fig. 7

Osteocytes is involved in bone formation-related gene expression in osteoblasts after ultrasound exposure. (A) MC3T3-E1 osteoblasts were cultured on the collagen gel with or without Ocy454 osteocytes. RNA samples were extracted from osteoblasts 1 hour after ultrasound exposure. The graphs show the mRNA expression of (B) Runx2, (C) Col1a1, (D) Alpl, and (E) Ocn in osteoblasts cultured with (Ocy-Ob) or without osteocytes (Ob). Data are presented as the median and interquartile range. n = 4 per group.

Fig. 8

Piezo1 knockdown in osteocytes attenuated bone formation-related gene expression in osteoblasts after ultrasound exposure. (A) Ocy454 osteocytes were transfected with control or Piezo1 siRNAs. siRNA-transfected Ocy454 cells were then embedded in the collagen gel, and native MC3T3-E1 cells were seeded onto the surface of the gel. RNA samples were extracted from osteocytes and osteoblasts 1 hour after ultrasound exposure. (B) The graph shows Piezo1 mRNA expression in osteocytes. The graphs show the mRNA expression of (C) Sost and (D) Dkk1 in osteocytes and (E) Runx2, (F) Col1a1, (G) Alpl, and (H) Ocn in osteoblasts. Data are presented as the median and interquartile range. n = 4 per group.

Fig. S1

Representative transverse and sagittal μCT images of fractured femurs on days (A) 7, (B) 21, and (C) 28 post-fracture are shown.

Fig. S2

(A) Representative alcian blue/picrosirius red-stained images of fractured femurs are shown. Scale bar = 500 μm. The graphs show (B) the fracture callus area and the percentage of (C) cartilage, (D) the newly formed bone, and (E) the fibrous area in the fracture callus. Data are presented as the median and interquartile range. n = 7-8 mice/group/time point.

Fig. S3

(A) Representative 3D images of the unfractured femur from GsMTx4-treated mice are shown. The graphs show (B) bone volume fraction (BV/TV) and (C) bone mineral density (BMD) of the unfractured femur. (D) The graph shows BV/TV in the fracture callus. (E) Representative alcian blue/picrosirius red-stained images of fractured femurs are shown.

Scale bar = 500 μm. The graphs show (F) the fracture callus area and the percentage of (G) cartilage, (H) the newly formed bone, and (I) the fibrous area in the fracture callus. (J) Representative TRAP-stained images of fractured femurs are shown. Scale bar = 100 μm. (K) The graphs show the percentage of TRAP-positive area in the fracture callus. (L) Representative immunostained images for type II collagen of fractured femurs are shown. Scale bar = 100 μm. (M) The graphs show the percentage of type II collagen-positive area in the fracture callus. (N) Representative immunostained images for type X collagen of fractured femurs are shown. Scale bar = 100 μm. (O) The graphs show the percentage of type X collagen-positive area in the fracture callus. Data are presented as the median and interquartile range. n = 5-6 mice/group.

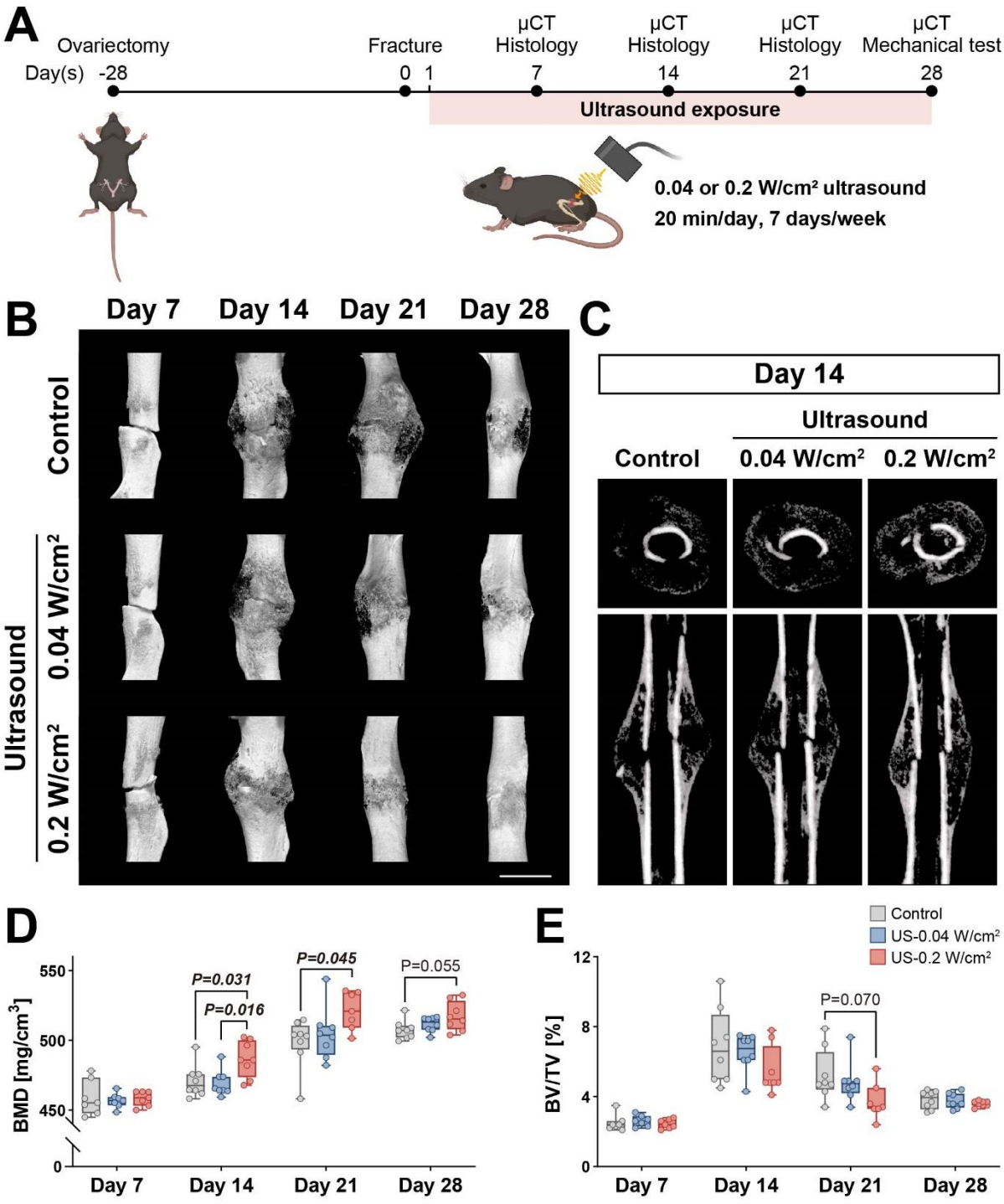
A
Ovariectomy
Day(s) -28
Fracture
0 1
μCT Histology
7
μCT Histology
14
μCT Histology
21
μCT Mechanical test
28
Ultrasound exposure
0.04 or 0.2 W/cm² ultrasound
20 min/day, 7 days/week
B
Day 7
Day 14
Day 21
Day 28
Control
Ultrasound
0.04 W/cm²
0.2 W/cm²
C
Day 14
Ultrasound
Control
0.04 W/cm²
0.2 W/cm²
D
BMD [mg/cm³]
550
500
450
0
P=0.031
P=0.016
P=0.045
P=0.055
Day 7
Day 14
Day 21
Day 28
E
Control
US-0.04 W/cm²
US-0.2 W/cm²
BV/TV [%]
12
8
4
0
P=0.070
Day 7
Day 14
Day 21
Day 28

Figure 1

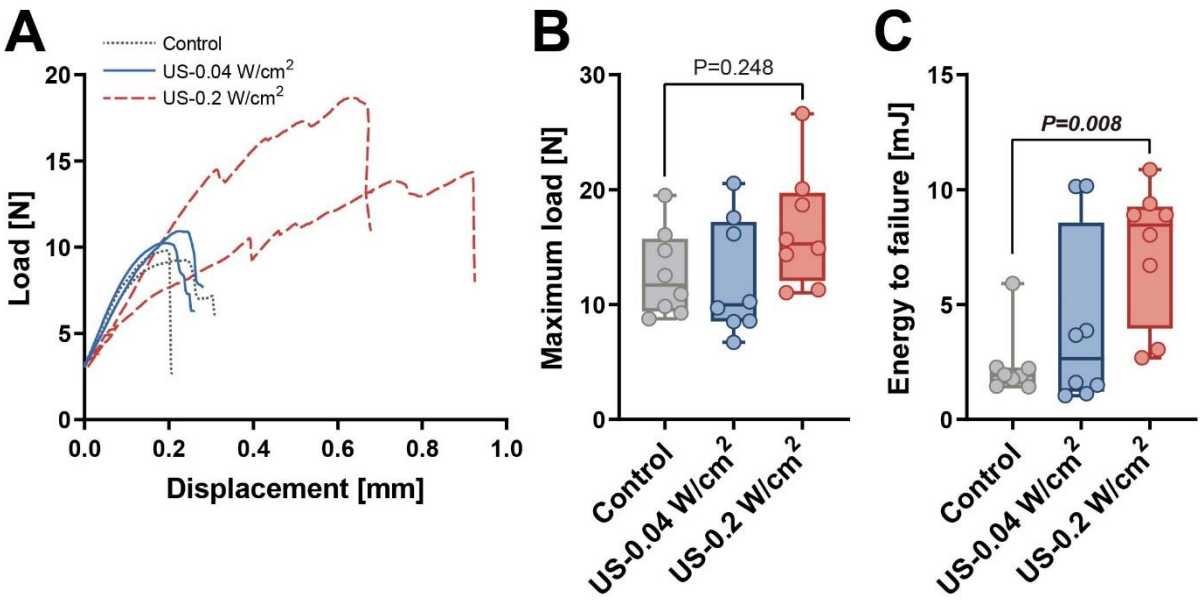
A
Control
US-0.04 W/cm2
US-0.2 W/cm2
Load [N]
Displacement [mm]
B
P=0.248
Maximum load [N]
Control
US-0.04 W/cm2
US-0.2 W/cm2
C
P=0.008
Energy to failure [mJ]
Control
US-0.04 W/cm2
US-0.2 W/cm2

Figure 2

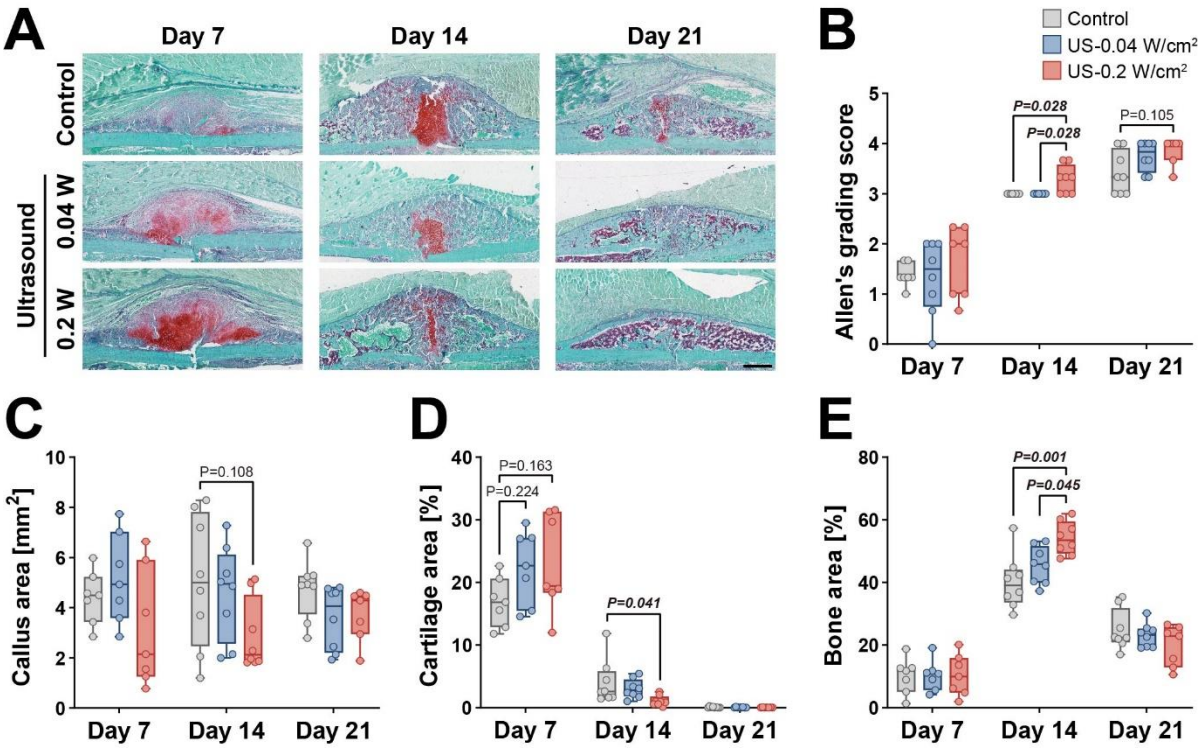
A
Day 7
Day 14
Day 21
Control
Ultrasound
0.04 W
0.2 W
B
Control
US-0.04 W/cm²
US-0.2 W/cm²
Allen's grading score
P=0.028
P=0.028
P=0.105
Day 7
Day 14
Day 21
C
Callus area [mm²]
P=0.108
Day 7
Day 14
Day 21
D
Cartilage area [%]
P=0.163
P=0.224
P=0.041
Day 7
Day 14
Day 21
E
Bone area [%]
P=0.001
P=0.045
Day 7
Day 14
Day 21

Figure 3

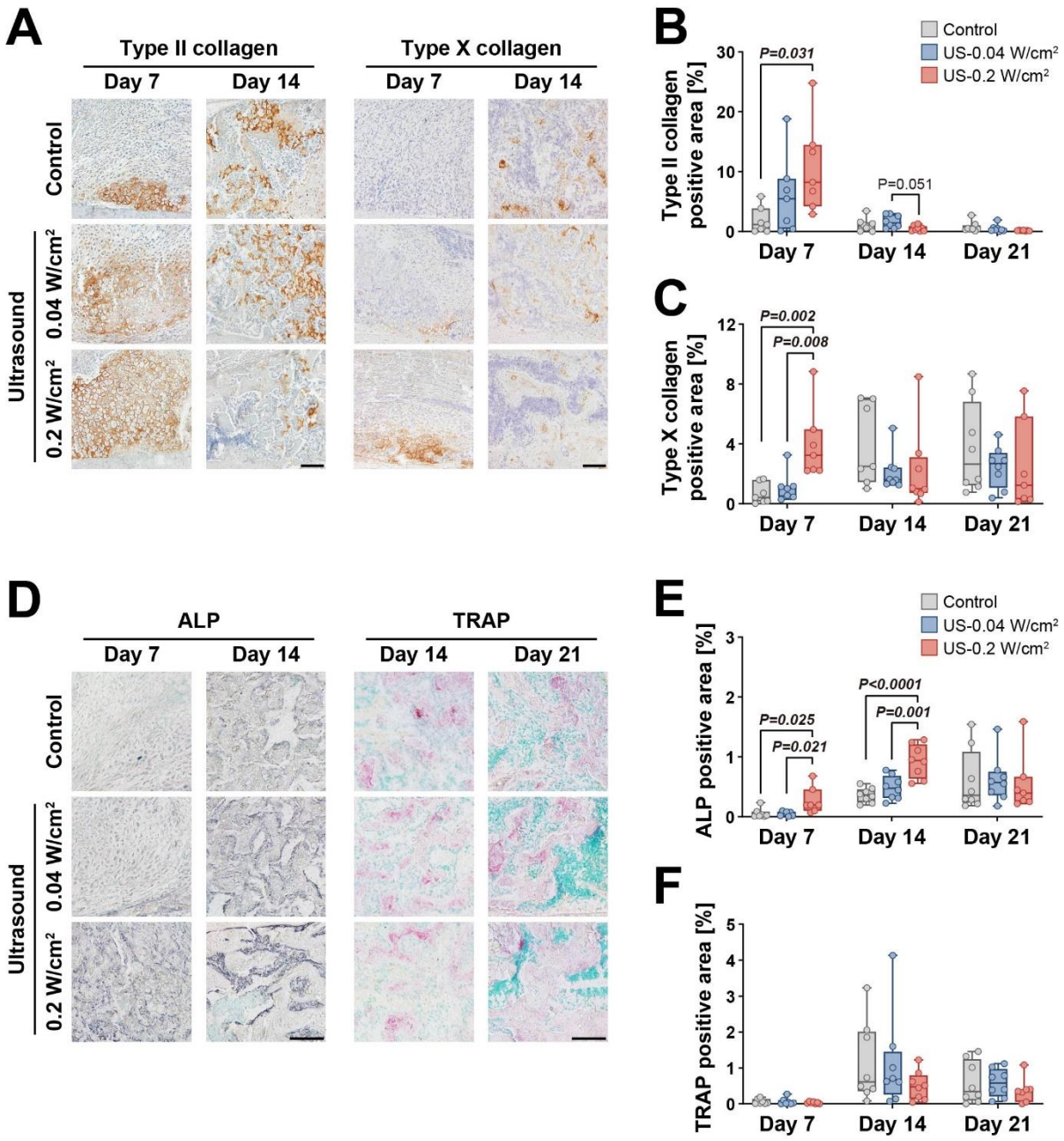
A
Type II collagen
Type X collagen
Day 7
Day 14
Day 7
Day 14
Control
Ultrasound
0.04 W/cm²
0.2 W/cm²
B
Control
US-0.04 W/cm²
US-0.2 W/cm²
Type II collagen positive area [%]
P=0.031
P=0.051
Day 7
Day 14
Day 21
C
Type X collagen positive area [%]
P=0.002
P=0.008
Day 7
Day 14
Day 21
D
ALP
TRAP
Day 7
Day 14
Day 14
Day 21
Control
Ultrasound
0.04 W/cm²
0.2 W/cm²
E
Control
US-0.04 W/cm²
US-0.2 W/cm²
ALP positive area [%]
P=0.025
P=0.021
P<0.0001
P=0.001
Day 7
Day 14
Day 21
F
TRAP positive area [%]
Day 7
Day 14
Day 21

Figure 4

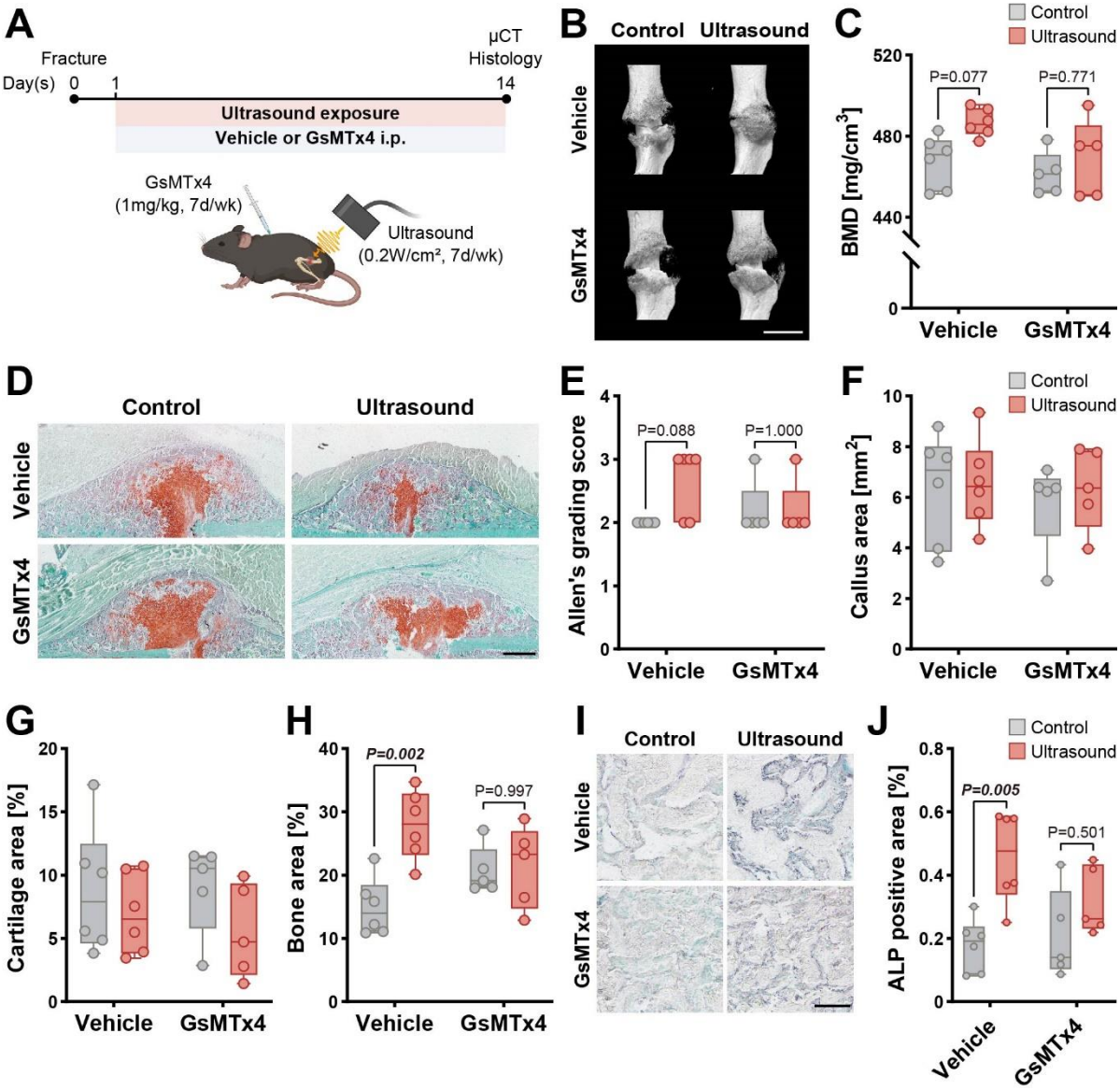
A
Fracture
Day(s) 0 1
μCT
Histology
14
Ultrasound exposure
Vehicle or GsMTx4 i.p.
GsMTx4
(1mg/kg, 7d/wk)
Ultrasound
(0.2W/cm², 7d/wk)
B
Control
Ultrasound
Vehicle
GsMTx4
C
Control
Ultrasound
BMD [mg/cm³]
520
480
440
0
P=0.077
P=0.771
Vehicle
GsMTx4
D
Control
Ultrasound
Vehicle
GsMTx4
E
Allen's grading score
P=0.088
P=1.000
Vehicle
GsMTx4
F
Control
Ultrasound
Callus area [mm²]
Vehicle
GsMTx4
G
Cartilage area [%]
Vehicle
GsMTx4
H
Bone area [%]
P=0.002
P=0.997
Vehicle
GsMTx4
I
Control
Ultrasound
Vehicle
GsMTx4
J
Control
Ultrasound
ALP positive area [%]
P=0.005
P=0.501
Vehicle
GsMTx4

Figure 5

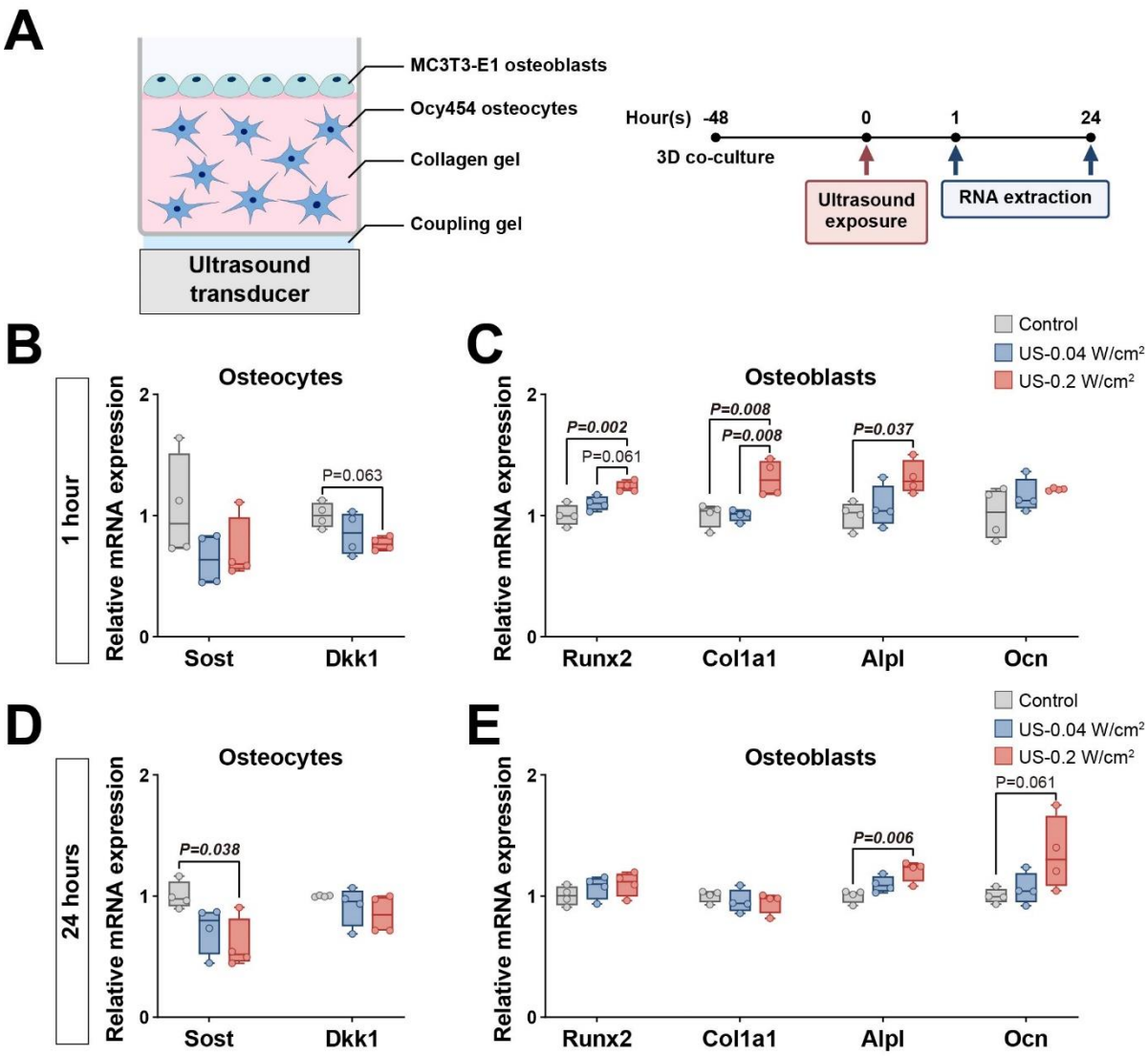
A
MC3T3-E1 osteoblasts
Ocy454 osteocytes
Collagen gel
Coupling gel
Ultrasound transducer
Hour(s) -48
0
1
24
3D co-culture
Ultrasound exposure
RNA extraction
B
1 hour
Osteocytes
Relative mRNA expression
P=0.063
Sost
Dkk1
C
Control
US-0.04 W/cm²
US-0.2 W/cm²
Osteoblasts
P=0.002
P=0.061
P=0.008
P=0.008
P=0.037
Runx2
Col1a1
Alpl
Ocn
D
24 hours
Osteocytes
P=0.038
E
Osteoblasts
P=0.006
P=0.061

Figure 6

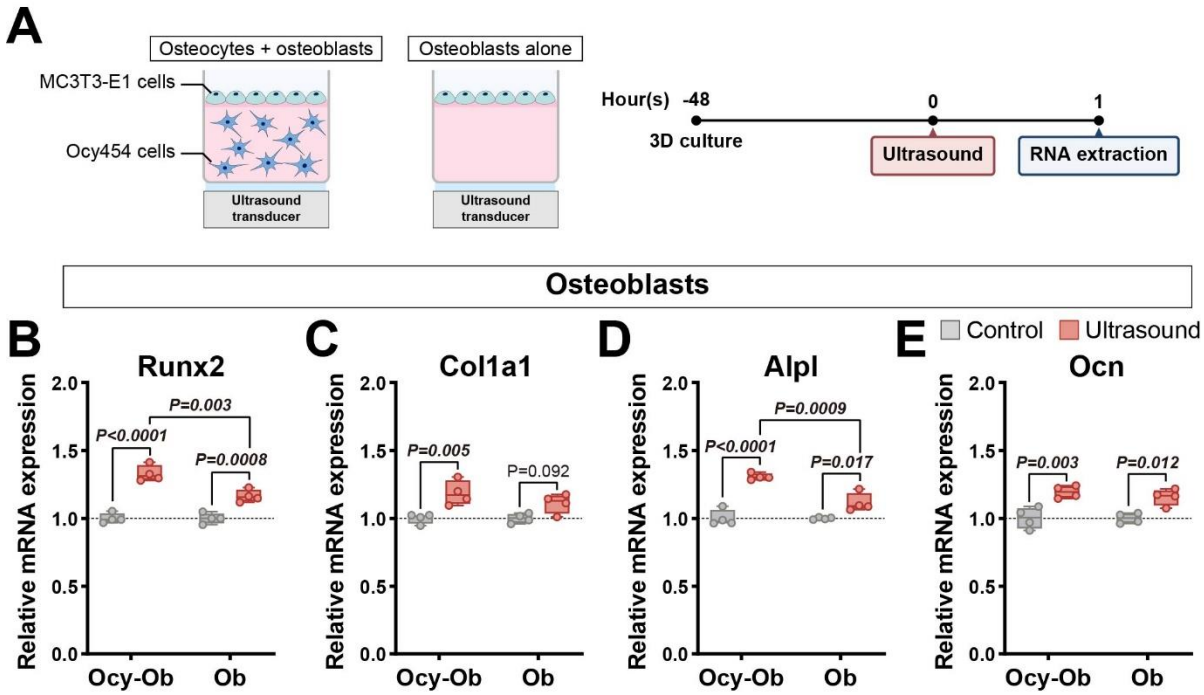
A
Osteocytes + osteoblasts
Osteoblasts alone
MC3T3-E1 cells
Ocy454 cells
Ultrasound transducer
Ultrasound transducer
Hour(s) -48
0
1
3D culture
Ultrasound
RNA extraction
Osteoblasts
B
Runx2
C
Col1a1
D
Alpl
E
Control
Ultrasound
Ocn
Relative mRNA expression
2.0
1.5
1.0
0.5
0.0
P<0.0001
P=0.003
P=0.0008
P=0.005
P=0.092
P<0.0001
P=0.0009
P=0.017
P=0.003
P=0.012
Ocy-Ob
Ob

Figure 7

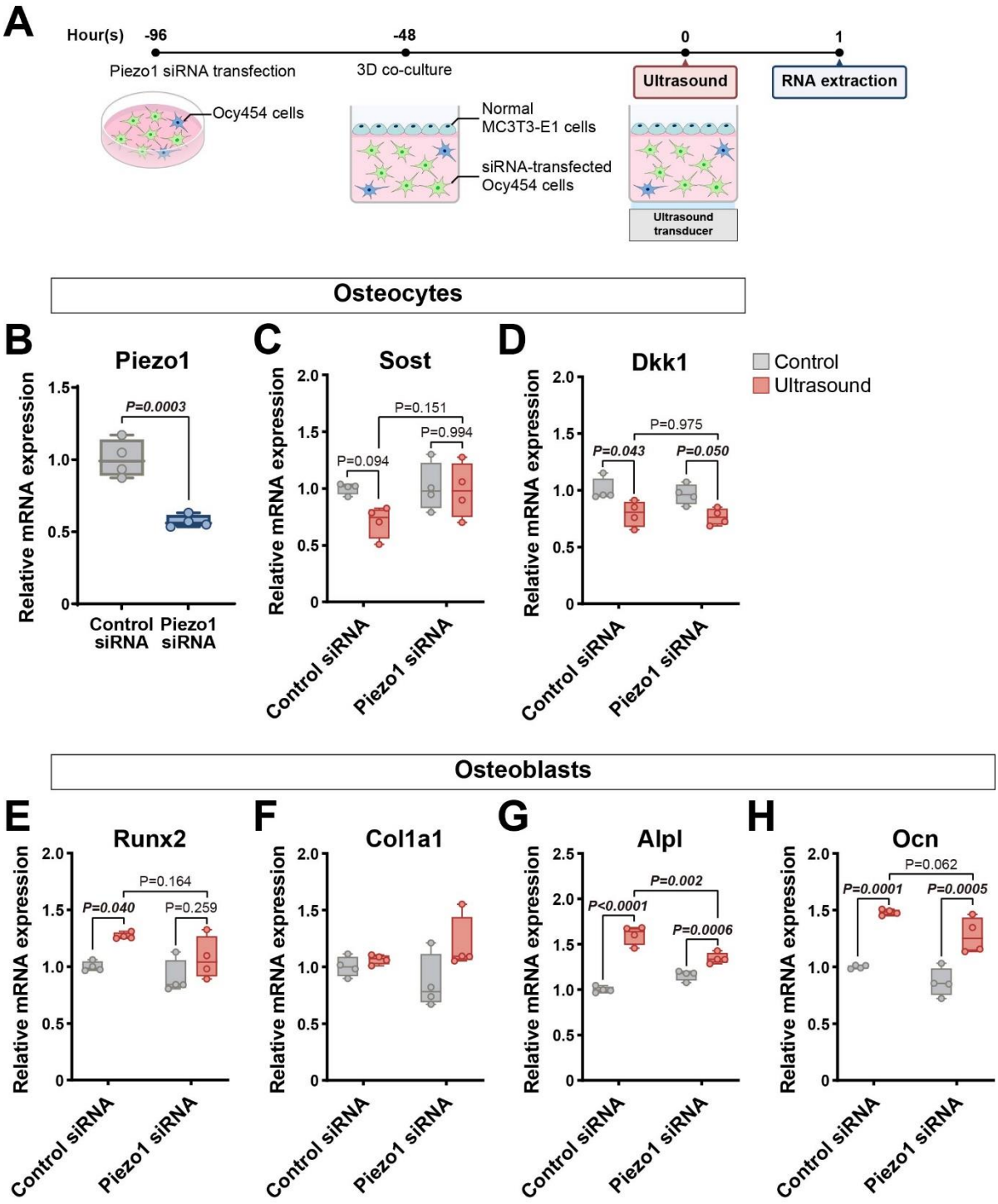
A
Hour(s)
-96
-48
0
1
Piezo1 siRNA transfection
3D co-culture
Ultrasound
RNA extraction
Ocy454 cells
Normal MC3T3-E1 cells
siRNA-transfected Ocy454 cells
Ultrasound transducer
Osteocytes
B
Piezo1
C
Sost
D
Dkk1
Control
Ultrasound
Relative mRNA expression
P=0.0003
Control siRNA
Piezo1 siRNA
P=0.094
P=0.151
P=0.994
P=0.043
P=0.975
P=0.050
Osteoblasts
E
Runx2
F
Col1a1
G
Alpl
H
Ocn
P=0.040
P=0.164
P=0.259
P<0.0001
P=0.002
P=0.0006
P=0.0001
P=0.062
P=0.0005

Figure 8

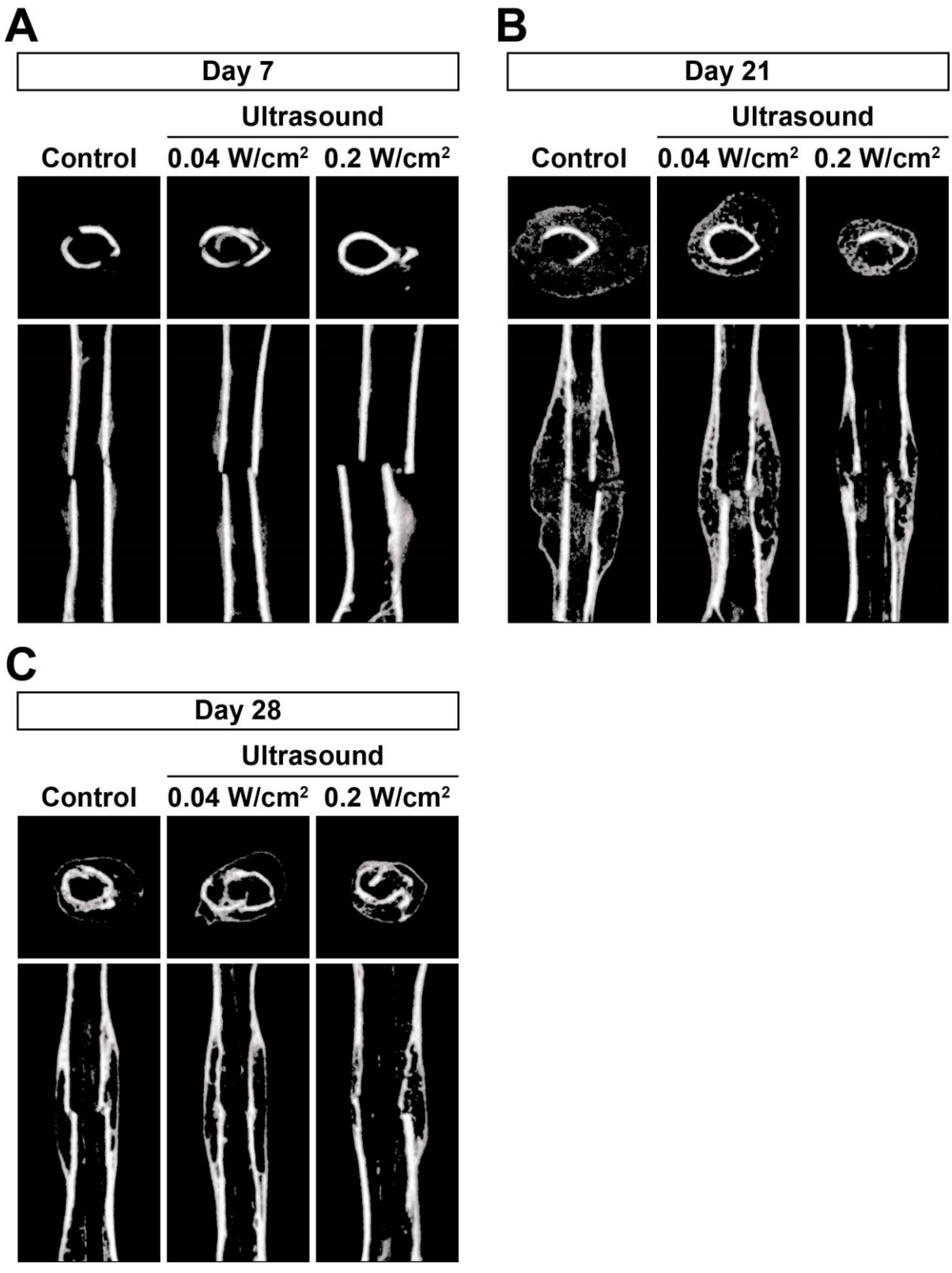
A
Day 7
Ultrasound
Control
0.04 W/cm²
0.2 W/cm²
B
Day 21
Ultrasound
Control
0.04 W/cm²
0.2 W/cm²
C
Day 28
Ultrasound
Control
0.04 W/cm²
0.2 W/cm²

Figure S1

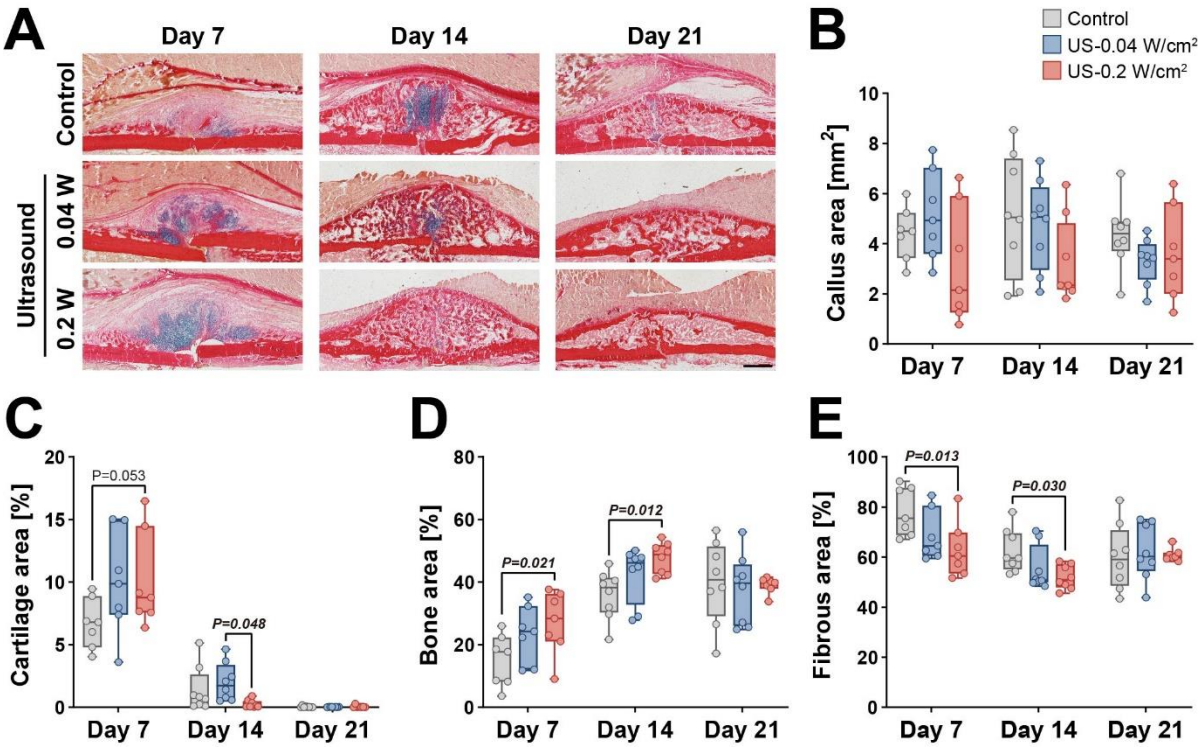
A
Day 7
Day 14
Day 21
Control
Ultrasound
0.04 W
0.2 W
B
Control
US-0.04 W/cm²
US-0.2 W/cm²
Callus area [mm²]
Day 7
Day 14
Day 21
C
Cartilage area [%]
P=0.053
P=0.048
D
Bone area [%]
P=0.021
P=0.012
E
Fibrous area [%]
P=0.013
P=0.030

Figure S2

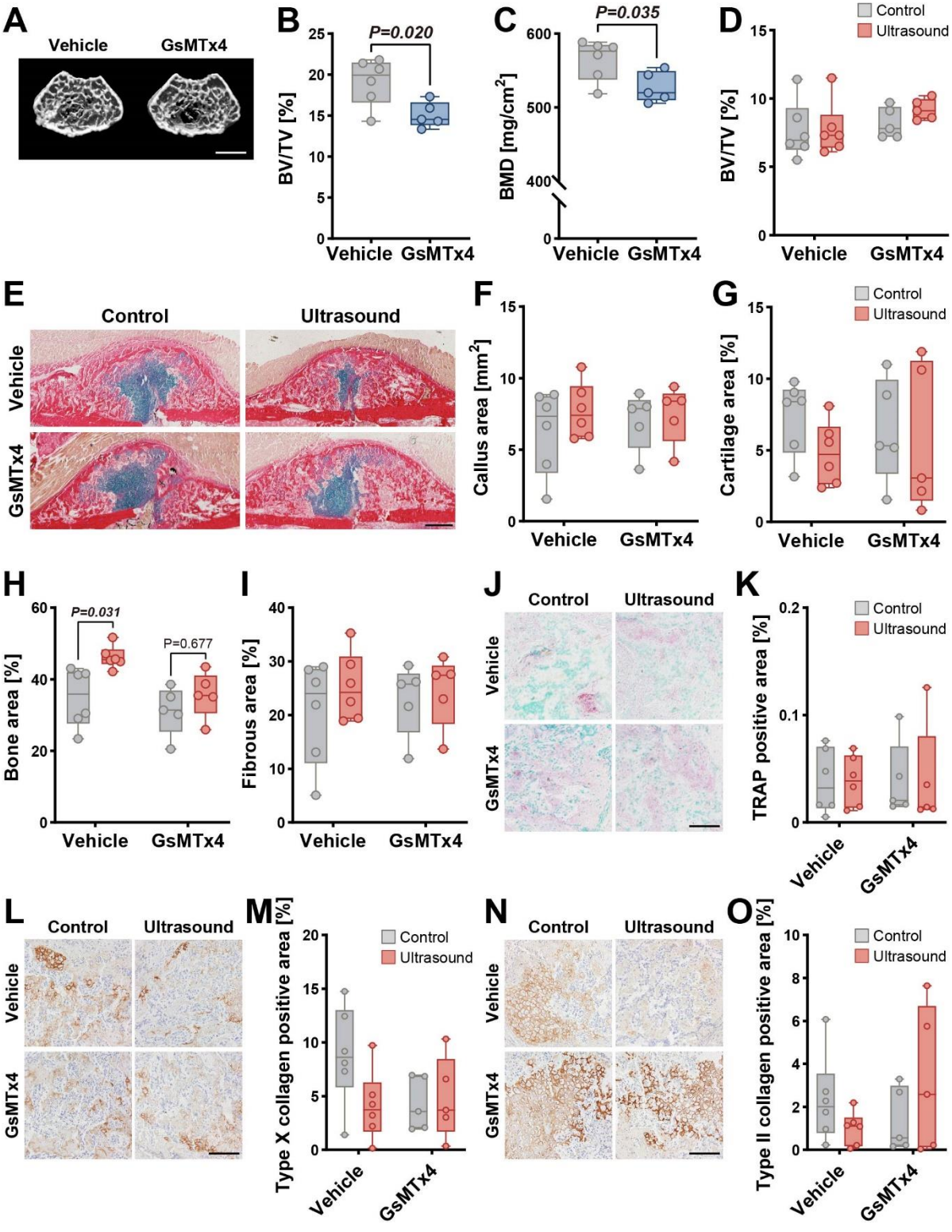
A
Vehicle
GsMTx4
B
P=0.020
BV/TV [%]
Vehicle
GsMTx4
C
P=0.035
BMD [mg/cm2]
Vehicle
GsMTx4
D
Control
Ultrasound
BV/TV [%]
Vehicle
GsMTx4
E
Control
Ultrasound
Vehicle
GsMTx4
F
Callus area [mm2]
Vehicle
GsMTx4
G
Control
Ultrasound
Cartilage area [%]
Vehicle
GsMTx4
H
P=0.031
P=0.677
Bone area [%]
Vehicle
GsMTx4
I
Fibrous area [%]
Vehicle
GsMTx4
J
Control
Ultrasound
Vehicle
GsMTx4
K
Control
Ultrasound
TRAP positive area [%]
Vehicle
GsMTx4
L
Control
Ultrasound
Vehicle
GsMTx4
M
Control
Ultrasound
Type X collagen positive area [%]
Vehicle
GsMTx4
N
Control
Ultrasound
Vehicle
GsMTx4
O
Control
Ultrasound
Type II collagen positive area [%]
Vehicle
GsMTx4

Figure S3